UCRL 17147

University of California

Ernest O. Lawrence Radiation Laboratory

ELECTRON TRANSFER IN WEAKLY IONIZED GASES

TWO-WEEK LOAN COPY

This is a Library Circulating Copy which may be borrowed for two weeks. For a personal retention copy, call Tech. Info. Division, Ext. 5545

Berkeley, California

DISCLAIMER

This document was prepared as an account of work sponsored by the United States Government. While this document is believed to contain correct information, neither the United States Government nor any agency thereof, nor the Regents of the University of California, nor any of their employees, makes any warranty, express or implied, or assumes any legal responsibility for the accuracy, completeness, or usefulness of any information, apparatus, product, or process disclosed, or represents that its use would not infringe privately owned rights. Reference herein to any specific commercial product, process, or service by its trade name, trademark, manufacturer, or otherwise, does not necessarily constitute or imply its endorsement, recommendation, or favoring by the United States Government or any agency thereof, or the Regents of the University of California. The views and opinions of authors expressed herein do not necessarily state or reflect those of the United States Government or any agency thereof or the Regents of the University of California.

UCRL-17147

UNIVERSITY OF CALIFORNIA

Lawrence Radiation Laboratory
Berkeley, California

AEC Contract No. W-7405-eng-48

ELECTRON TRANSFER IN WEAKLY IONIZED GASES

Eric Keith Parks

(Ph.D. Thesis)

September 1966

TABLE OF CONTENTS

ABSTRACT

I INTRODUCTION 1

II EXPERIMENTAL APPARATUS AND PROCEDURE 3

A. Apparatus 3

1. Reaction Cell and Oven 3

2. Light Source 6

3. Collection Voltage 7

4. Experimental Errors 9

B. Systems Studied 10

1. Thallium Halides 10

2. The Use of Inert Gases 10

3. Experiments with Nitrogen Dioxide 12

III EXPERIMENTAL RESULTS 17

A. Decay Processes 17

B. Numerical Determination of Recombination and Diffusion Constants 23

1. Ambipolar Diffusion 23

2. Experimental Diffusion Constants and Recombination Coefficients 30

C. Temperature Dependence of the Recombination Coefficient 38

IV NATURE OF THE IONIZED GAS 42

A. Mass Spectrometry 42

1. Mass Spectrometer 43

2. Light Source 46

3. Results 48

B. Estimates of Complex Formation 56

1. Ion-parent Molecule Complexes 56

2. Ion Neutral Complexes 60

3. Rate Constants 62

C. Diffusion Constants 64

V THEORY OF IONIC RECOMBINATION AND COMPARISON WITH EXPERIMENT 73

A. Mechanisms of Ionic Recombination 73

B. Three Body Recombination 74

1. Mechanism 74

2. Determination of the Capture Radius 75

3. Rate Constant 84

C. Two-Body Recombination 89

Acknowledgments 96

The theory based on the Thomson model for three body recombination is extended to ions of different masses and the resulting predicted rate constants are consistantly well below experimental results. The reasons for these discrepancies are discussed.

Bruce H Mahan

I. INTRODUCTION

The neutralization of a gas of positive and negative ions, commonly called ion-ion recombination, takes place primarily by a collisional electron transfer process. Because of the strong Coulomb attraction the rates of such processes are several orders of magnitude larger than typical bimolecular reactions among neutral species. In the absence of an inert background gas the reaction is bimolecular and may be written

$$X^+ + Y^- \rightarrow X^* + Y^* \qquad (I.1)$$

where X and Y may be atoms or molecules and the asterisk indicates that the products may depart in excited states. The addition of a background gas, necessary experimentally to limit the large ion losses due to diffusion, increases the recombination rate through three body interactions.

The theoretical tools available for the calculation of the two and three body rates are quite meager. There is little hope of obtaining quantitative theoretical estimates of two body recombination rates (Eq. (I.1)) until detailed calculation of the potential curves for the reacting species are available. The mechanism of three body recombination is generally thought to be understood, but recently there has been much criticism[1,2] of the apparent success of earlier theoretical results.

We report here two and three body recombination rates of the ions formed from the photolysis of thallium halide vapors. Chapters II and III discuss the method used and the experimental results, chapter IV deals with the nature of the ions present in the experiments, and chapter V presents the current state of the theory and a comparison with the experimental results.

References for Chapter I

1. K. A. Brueckner, J. Chem. Phys. 40, 439 (1964).

2. P. J. Feibelman, J. Chem. Phys. 42, 2462 (1965).

II. EXPERIMENTAL APPARATUS AND PROCEDURE

The measurement of the rate loss of positive and negative ions in a weakly ionized gas was made by the following method. The ions were formed between parallel plate collection electrodes by photoionization from a condensed spark. The ions disappeared by recombination and diffusion to the electrodes. At various delay times from the initial spark a potential was applied at the electrodes and the ions remaining were collected. The charge collected was determined by integrating the voltage produced across a known resistor. By repeating the experiment at various delay times, an ion loss curve could be obtained from which a numerical analysis determined the important recombination and diffusion parameters.

A. Apparatus

1. Reaction Cell and Oven

The thallium halides require heating (500-600°K) to produce a sufficiently high vapor pressure (one to ten microns). The reaction cell was a 90 mm o.d. quartz tube 10.4 cm long with optical quartz plate windows (~25 mm diameter) axially located at each end. The high voltage plate was 48×58 mm^2 and was 20 mm from the 15×25 mm^2 collecting plate, which was centered in a 18×28 mm^2 hole in a 48×58 mm^2 guard ring. The plates and guard ring were made of nickel and were spot welded to tungsten wires which passed to the outside through tungsten to pyrex seals. The inner surface of the reaction cell was coated with a conducting layer of colloidal graphite (Aquadag), which was connected to an external electrode so that the walls of the cell could be maintained at ground potential.

The reaction cell was enclosed in a $15.5 \times 18 \times 21$ cm^3 aluminum box which itself was enclosed in a transite oven. The aluminum box served the dual purpose of keeping out stray fields and keeping the temperature uniform within the box. The heaters for the oven were placed between the transite and the aluminum. Both the aluminum box and transite oven had windows on either end to allow the ionizing radiation to enter and leave the cell. The sample was contained in a tube which extended from the base of the cell through the bottom of the oven and into a brass tube, separately heated and temperature regulated by a Hallikainen Thermotrol unit which has a temperature sensitivity of .001°C. The main oven was kept 20-50°C hotter than the sample temperature in order to prevent vapor from condensing on the cell windows. A magnetically actuated ground glass seal prevented the sample vapor from condensing onto the cold parts of the apparatus. The tungsten leads from the cell were led out of the oven through ceramically insulated brass tubes which led into standard electrical fittings and cable.

The set of electrodes had been previously used[1] in another cell at which time an analog field plotter was used to determine the equipotential lines in the reaction cell, and the flux lines indicated that the effective volume from which ions were collected was $14.3 \times 23.7 \times 20$ mm^3, or 6.77 cm^3. Figure 1 shows a side view of the equipotential lines and the flux lines.

The cell was connected to a conventional vacuum system which used an oil diffusion pump. A cold trap prevented mercury vapor from entering the cell from the manometer used to read the total gas pressure. Stopcocks were greased with Apiezon N grease except for the experiments with nitrogen dioxide in which case Dow-Corning silicone grease was used.

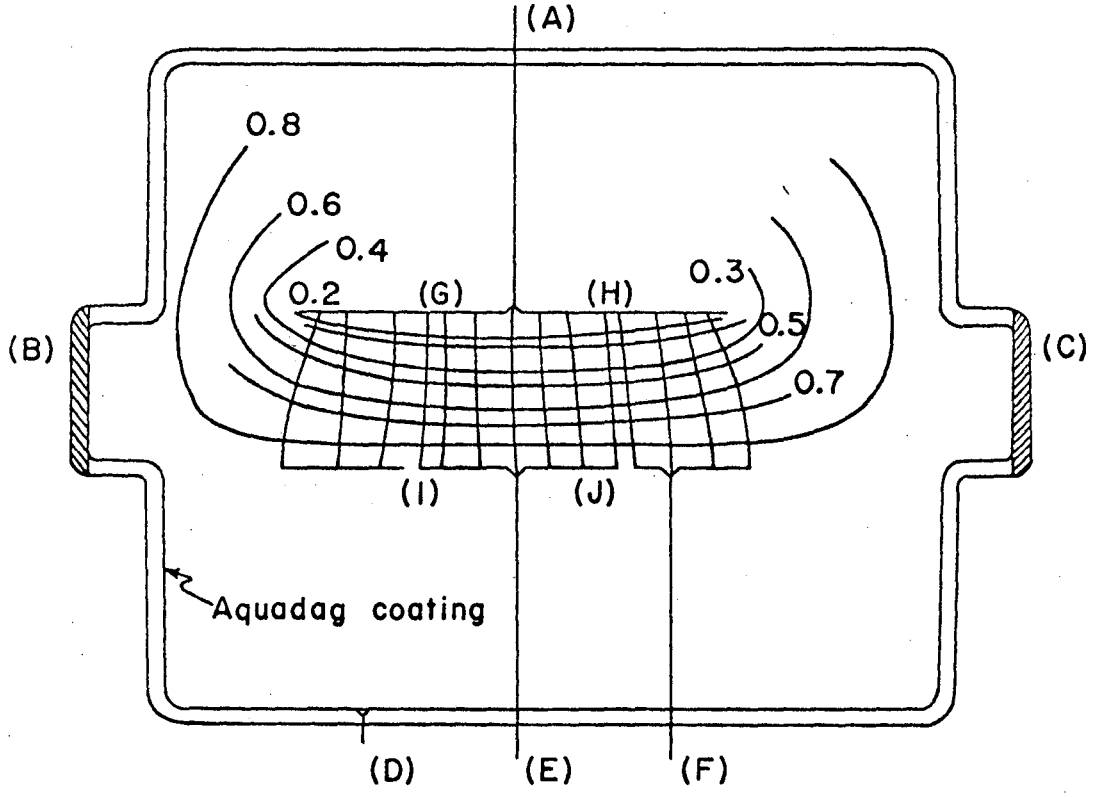

Fig. 1 Side view of equipotential surfaces and flux lines in reaction cell: (A) High-voltage terminal; (B) Quartz window to spark source; (C) Quartz window to photomultiplier; (D) Aquadag-coating terminal; (E) Collecting-plate terminal; (F) Guard-ring terminal; (GHIJ) Cross section of actual collection volume.

2. Light Source

The work of Terenin and Popov[2] indicates that the radiation from a condensed spark between electrodes of various metals (Zn, Al, Cd) would produce photoionization of the thallium halides. The spark source was chosen for the recombination experiments since it proved to be a fairly reproducible, high intensity source of light of sufficiently short duration so as not to interfere with the recombination process.

The electrodes were housed in a grounded rectangular copper box and were connected to the power source through coaxial cable to limit radiation interference. A window fitted with quartz plate was situated on one side of the box about 2.5 cm from the electrode gap and the copper box was placed flush with the oven. The distance from the electrode gap to the middle of the collection electrodes was about 14 cm. Three quartz windows separated the electrodes from the ionizing region within the cell. A 1 mfd capacitor was charged to 6000-8000 volts and discharged through a thyratron tube from a switch on the front of the power supply. The copper electrode box was flushed continuously with inert gas to reduce the breakdown voltage across the electrode gap.

It was found that argon not only decreased the breakdown voltage more than helium but also resulted in an increase in ionizing radiation by a factor of 4-5. This is probably due mainly to the presence of strong argon emission lines in the region of 1800-1900 Å. The photoionization spectrum was appreciable in this region for each of the three halides.[2] The additional intensity was needed to increase the predominance of recombination loss to diffusion loss and in the case of thallium chloride, which is the least photosensitive of the thallium halides, it was needed to make the experiment possible at all.

A photomultiplier was placed outside the exit window of the oven and served to trigger the type 555 Tektronix oscilloscope as well as provide a monitor for the light intensity. The oven window was blackened with carbon so as not to overload the photomultiplier. The output voltage of the photomultiplier was connected to one of the operational amplifier inputs of a type O Tektronix operational amplifier plug-in unit functioning as an integrator.

3. Collection Voltage

The collection voltage was obtained using the circuit shown in Fig. 2. The circuit is designed to eliminate the transient current produced by the application of the collection voltage. The first part is a univibrator[3] which converts the two volt one microsecond delayed trigger pulse from the oscilloscope into a ten volt square pulse the duration of which is determined by the capacitor C. In these experiments, C was equal to 0.0143μf which gave a five millisecond pulse. The ten volt square pulse is amplified into two 200 volt square pulses of opposite polarity. One pulse is applied to the high voltage electrode of the cell and the other to one side of a variable capacitor. The capacitor was two 2 cm^2 copper plates mounted in an aluminum box. By varying the separation of the plates the capacitance of the cell could be matched and the application of the collection voltage to the cell then produced no voltage change at the collection electrode.

While the photomultiplier output voltage served as a trigger for the time base of the oscilloscope it was found that the noise of the spark discharge in general also triggered the oscilloscope. This would not have been significant, since the electrical disturbance was of very short duration (~1 microsec.) except for the fact that the noise also

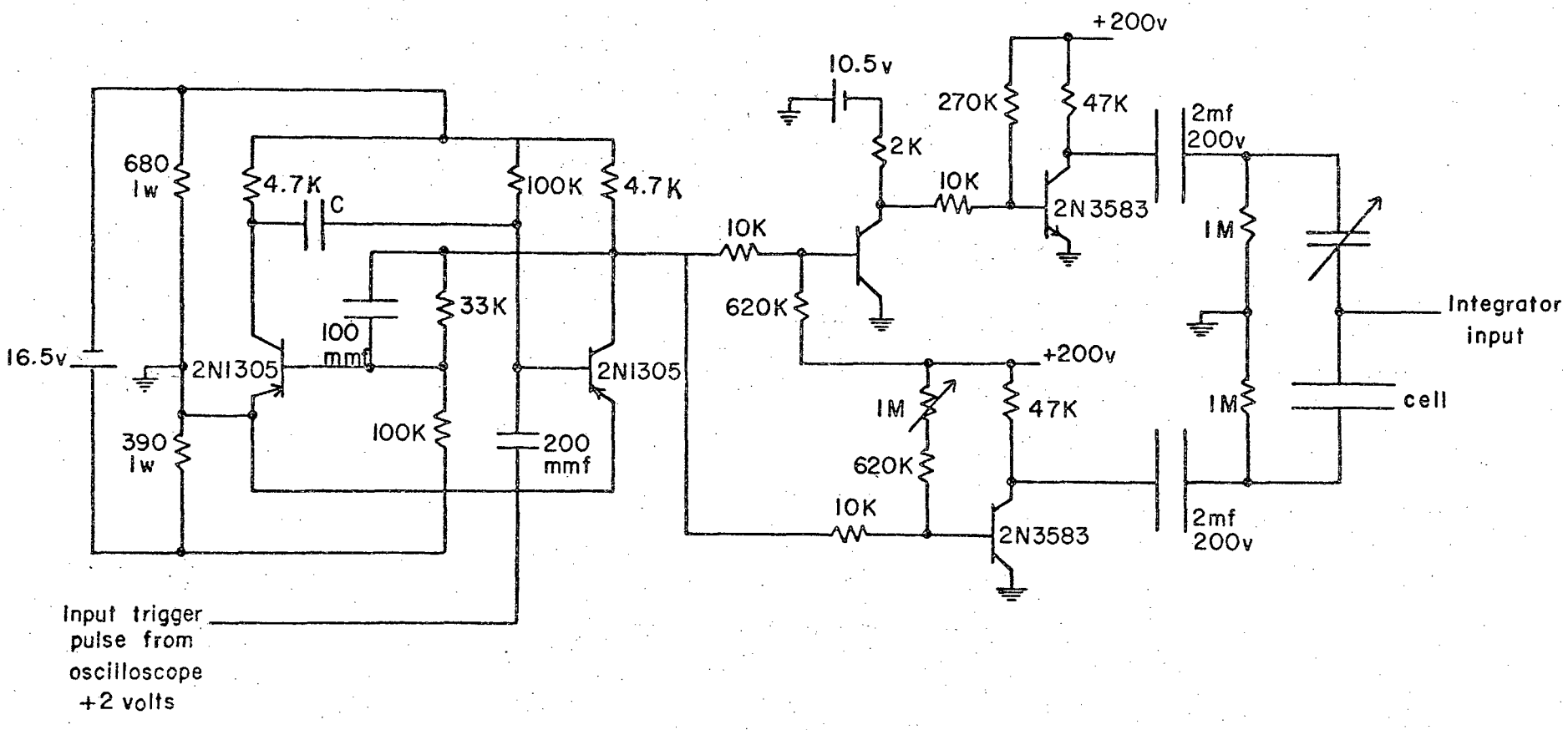

Fig. 2 Collection voltage circuit triggered from the delayed trigger pulse on the 555 Tektronix oscilloscope

triggered the univibrator which then applied the collection voltage prematurely. The problem seemed insensitive to any shielding that was applied and its occurrence seemed to depend on which of several thyratron tubes were employed. The problem was essentially eliminated by using batteries for the biasing potentials in Fig. 2 and a rather careful positioning of the components.

4. Experimental Errors

The area under the collection curve was compared with the value obtained from the integrator for several points and agreement was within a few percent.

In an actual experiment the integrated photomultiplier voltage and integrated collection voltage were simultaneously displayed on the oscilloscope. All voltages were read directly from the oscilloscope. Only those data were used for which the integrated photomultiplier voltage was equal to a previously chosen standard. Errors resulted from the difficulty in obtaining exactly reproducible spark intensities and also difficulty in reading the small collection voltages (~2-10 millivolts) at the long delay times. The latter difficulty resulted in the long time, low density points being more scattered, although the resulting effect on the determination of the recombination coefficient was very small. The difficulty in obtaining reproducible ionizing radiation also added to the scatter and this was one of the main difficulties in determining the recombination coefficient from a given curve.

Drift in the initial ion density for a given spark intensity was a frequent source of difficulty. In some cases, this was due to a lack of temperature equilibrium, but in many cases there was no apparent ex-

planation for the drift. While frequent check was made at small delay times to insure that the initial ion density had not changed during a given run some of the rate curves indicated that such a change had occurred. This may have been the chief source of errors in the experiment. In the absence of diffusion such an effect would be easily seen, however the curvature of the plots due to diffusion loss made it difficult to see the effect of the drift.

B. Systems Studied

1. Thallium Halides

The experiments reported here were done on the vapors of thallium iodide, thallium bromide, and thallium chloride. Experiments were also done with thallium iodide in the presence of nitrogen dioxide. Inert gas was present in all experiments from 35-400 torr.

The thallium halides were obtained from Cooper Chemical Company, Long Valley, New Jersey. The stated purity was 99.9% min. Thallium iodide was the most photosensitive and could be studied at the lowest temperature, 530°K. The bromide and chloride were heated to approximately 590°K and 610°K respectively and the thallium iodide, nitrogen dioxide experiments were done at 550°K. Vapor pressures at various temperatures are given in Fig. 3 from data given by Barrow, Jeffries, and Swinstead.[4]

2. The Use of Inert Gases

The presence of inert gas is necessary not only to determine the three body pressure dependence of the rate, but also to limit sufficiently the diffusional loss. At low third body pressures, diffusion dominates and it becomes difficult to separate the small recombination part of what is essentially an exponential diffusion loss curve. In these experiments

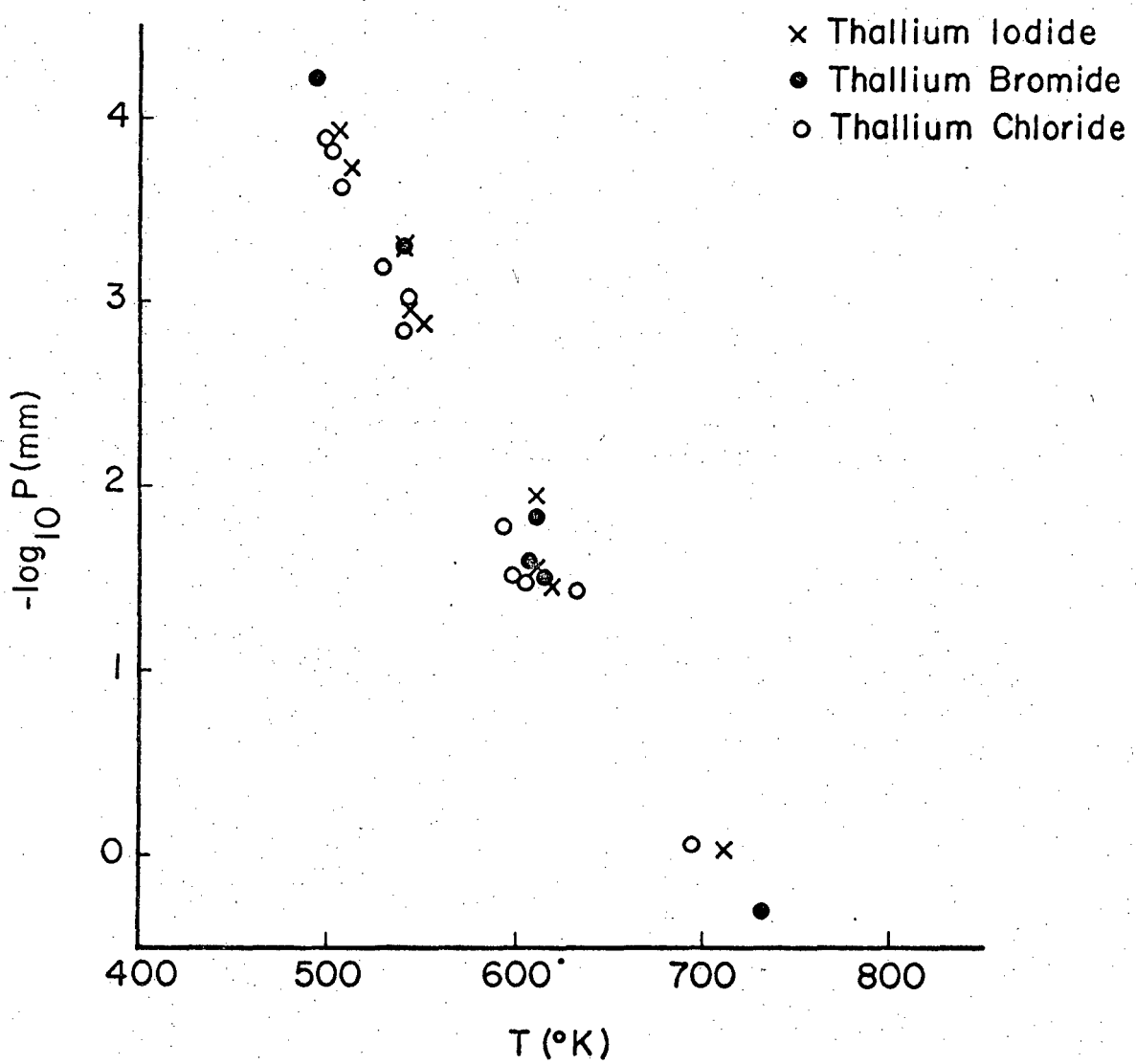

Fig. 3 Plot of $-\log_{10}$ (pressure) vs temperature for the thallium halides

this required a minimum third body pressure of about 35 torr (no. density = 5.8×10^{17} at T = 580°K).

Argon and xenon were the inert gases used in these experiments. Since the pressure dependence obtained with argon was quite small, experiments with lighter inert gases were not attempted. Argon was obtained in cylinder tanks from Air Reduction Company. It was used without further purification and was not reused after each experiment. Xenon was supplied by Air Reduction Company in Pyrex flasks and was also not further purified. It was pumped on and distilled from an isopentane slush bath at -160°C, after use in several experiments but was not reused after the experiments with nitrogen dioxide.

The upper limit to the neutral gas pressure was determined by the ion collection time. A collection voltage of 200 volts was used in all experiments to collect the ions. At pressures above 225 torr for xenon and about 400 torr for argon, the ion collection curves, which are illustrated in Fig. 4, cut off at 4-5 milliseconds. Since ions recombine during the collection process, long collection times mean that the ion concentration will appear too low. At the highest pressures used the ions that recombined during collection were usually less than 10% of the ions present and this would not change the observed rate constant by more than a few percent.[5]

3. Experiments with Nitrogen Dioxide

Experiments were done with thallium iodide in the presence of nitrogen dioxide with the hope of studying the recombination of Tl^+ and NO_2^-. This requires that the reaction

$$I^- + NO_2 \rightarrow I + NO_2^- \qquad (11.1)$$

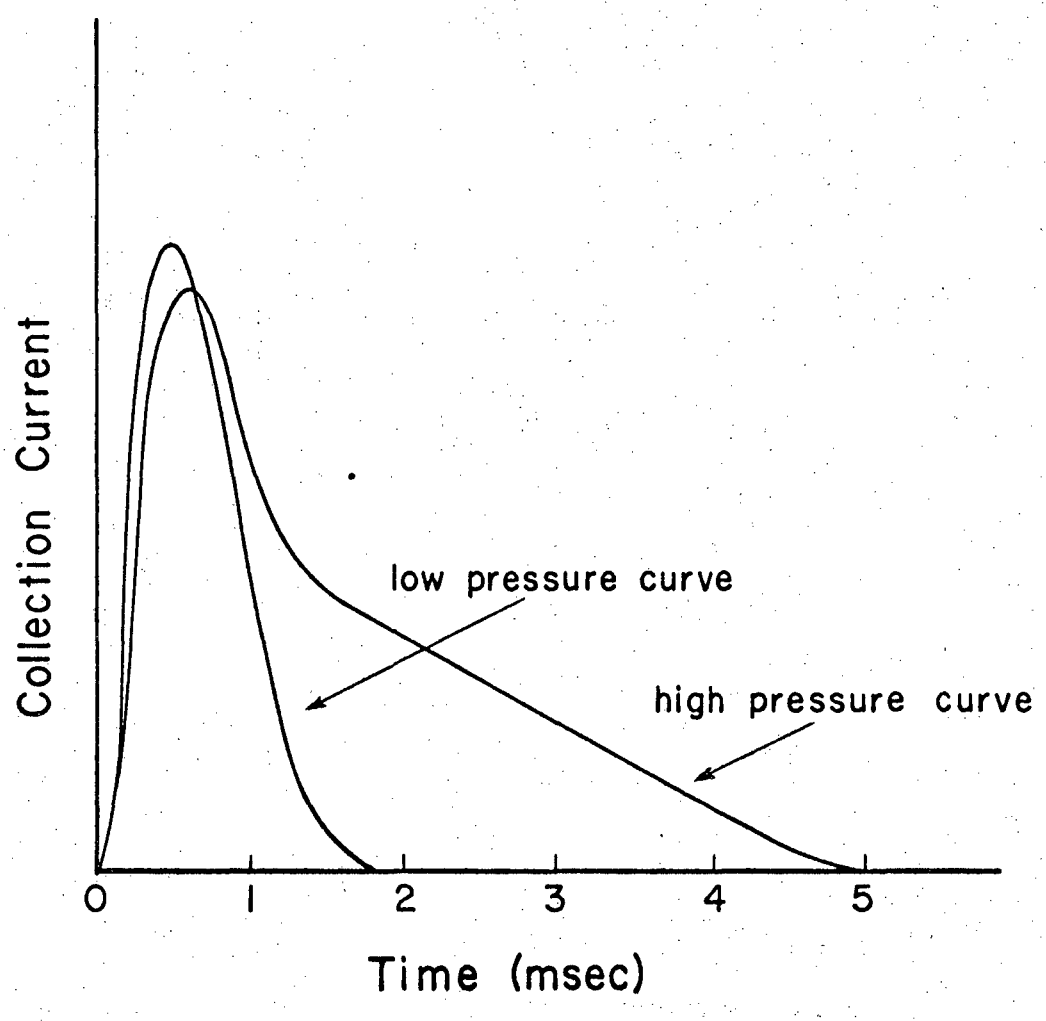

Fig. 4 Collection current vs time

be essentially complete and proceed much more rapidly than the recombination process. The equilibrium constant for the above reaction

$$K = \frac{[I][NO_2^-]}{[I^-][NO_2]} \tag{II.2}$$

is nearly equal to $\exp(\Delta A/kT)$ where ΔA is the difference between the electron affinities of $I(3.063\pm.003$ ev)[6] and $NO_2(4.0\pm.2$ ev).[7] With $T = 550°K$, $[I] = [NO_2^-]$, $[I] + [I^-] = 10^9$ ions/cm^3 and $[NO_2] = 10^{15}$ions/cm^3, we have

$$K = \frac{(10^9 - [I^-])^2}{[I^-] \times 10^{15}} = \exp(.94\times1.602\times10^{-12}/k\times550) = 4\times10^8 \tag{II.3}$$

and

$$\frac{[NO_2^-]}{[I^-]} = 4\times10^{14} \tag{II.4}$$

Consequently at equilibrium essentially all the negative ions are present as NO_2^-. Equilibrium however, is never attained and we must consider the kinetics of the charge exchange reaction.

The rate constant for the charge exchange reaction

$$O^+ + O_2 \rightarrow O_2^+ + O \tag{II.5}$$

is[8] $k = 2.5\times10^{-11}$ cm^3/sec. Using this value to get a rough estimate of the rate of formation of NO_2^-, we have

$$\frac{d[NO_2^-]}{dt} = 2.5\times10^{-11}[NO_2][I^-] \ . \tag{II.6}$$

With $(NO_2) = 10^{15}$ ions/cm^3,

$$\frac{d[NO_2^-]}{dt} = 2.5\times10^4\times[I^-] \text{ cm}^{-3}\text{sec}^{-1}. \tag{II.7}$$

Thus the reaction should be complete in a few tenths of a millisecond.

The results of the mass spectrometer experiments discussed in Chapter IV indicate that NO_2^- is not present in any detectable quantity when thallium iodide is photolyzed in the presence of nitrogen dioxide. Instead a rapid conversion of I^- into NO_3^- is observed. A discussion of the ions present in the nitrogen dioxide experiments is given in Chapter IV.

The nitrogen dioxide was made from cylinder grade nitric oxide and cylinder grade oxygen. The nitrogen dioxide was pumped on at -183°C, to remove any remaining oxygen. The pressure in the experiments was about 75μ.

References for Chapter II

1. J. C. Person, Mutual Charge Neutralization of Gaseous Ions (Ph.D. Thesis) University of California. Radiation Laborabory Report UCRL-10904, July 1963 (unpublished) p. 16.
2. A. Terenin and B. Popov, Phys. Z. Sow. 2, 299 (1932).
3. E. J. Bair, Introduction to Chemical Instrumentation (McGraw-Hill Book Co., New York, 1962) p. 183.
4. R. F. Barrow, E. A. N. S. Jeffries, and J. M. Swinstead, Trans. Faraday Soc. 51, 1650 (1956).
5. J. C. Person, Mutual Charge Neutralization of Gaseous Ions (Ph.D. Thesis) University of California Radiation Laboratory Report UCRL-10904, July 1963 (unpublished) p. 14.
6. R. S. Berry and C. W. Reimann, J. Chem. Phys. 38, 1540 (1963).
7. A. L. Farragher, F. M. Page, and R. C. Wheeler, Discussions of the Faraday Soc. 37, 203 (1964).
8. P. H. G. Dickinson and J. Sayers, Proc. Phys. Soc. (London) 76, 137 (1960).

III. EXPERIMENTAL RESULTS

A. Decay Processes

Ions can disappear by both diffusion to the electrodes and recombination. It is usually necessary from a mathematical point of view to assume that ions which strike a surface remain there and are neutralized by ions of the opposite charge. While this is probably not a good approximation for uncharged species, ions may be expected to interact strongly with the surface and remain bound there. A further approximation of charge neutrality is justified since small net charge differences produce large fields which prohibit further separation of charge. In the density range 2×10^8 to 4×10^6 ions/cc these fields limit net charge densities to .1 -.4% for Tl^+, I^- in Xe at 531°K (see Section B).

If the effect of diffusion is neglected, the rate equation for recombination is

$$-\frac{dn}{dt} = \alpha n^2 \qquad n = n^+ = n^- \qquad \text{(III.1)}$$

where n is the charge density, t is the time, and α is the recombination coefficient. The integrated form of the equation is

$$\frac{1}{n} = \frac{1}{n_o} + \alpha t \qquad \text{(III.2)}$$

Thus a plot of 1/n vs t should be linear with the slope giving the value of α. Examples of four such plots are given in Figs. 5-8. A high and low pressure plot is shown for the system Tl^+, I^- in both Xe and Ar. It should be noted that in these plots, the averaged ion density as determined from experiment is used, i.e., $n = \int n dV/V$.

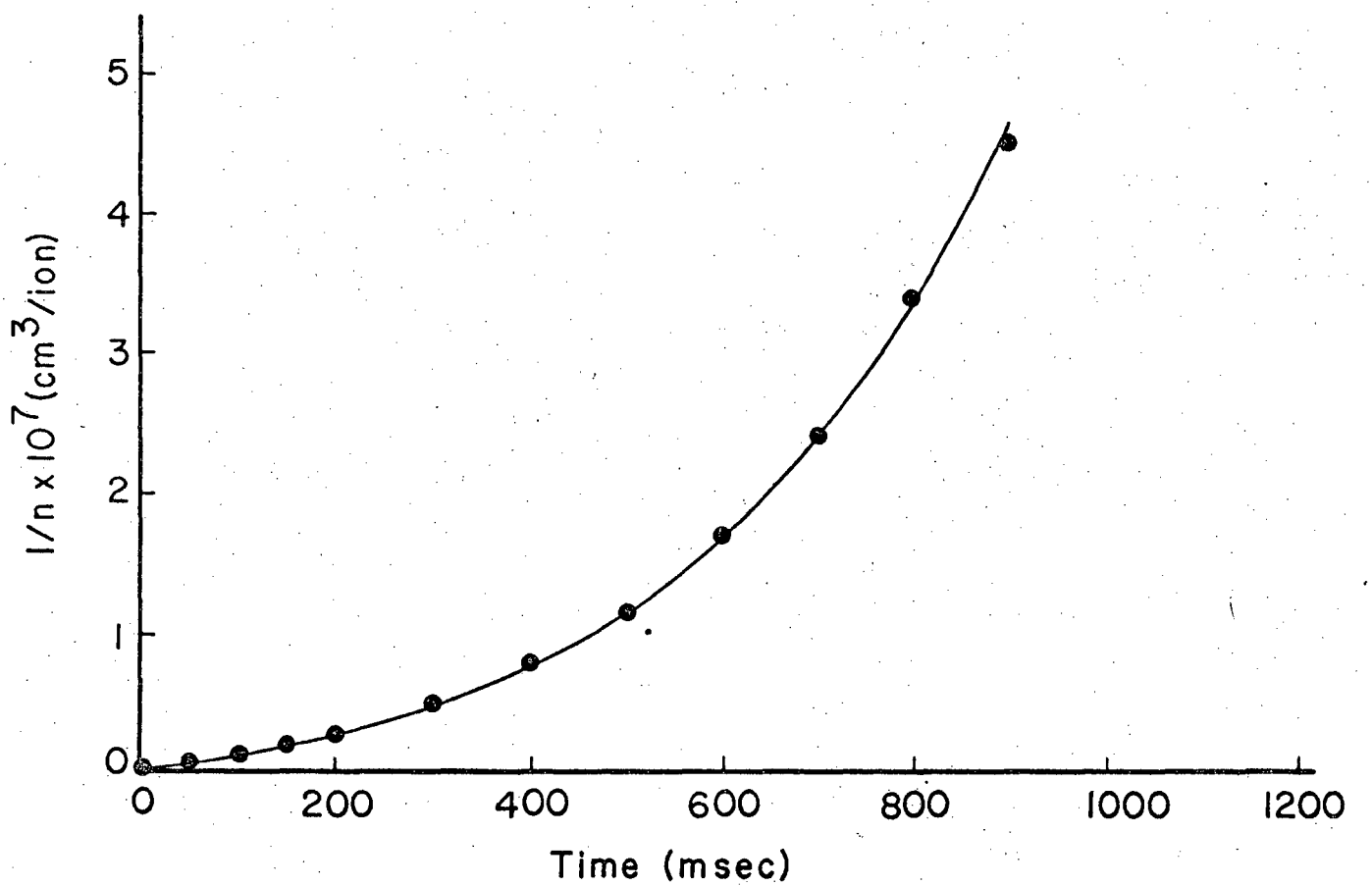

Fig. 5 Plot of 1/n vs time. TlI-Xe at 34 torr. n is the average ion density

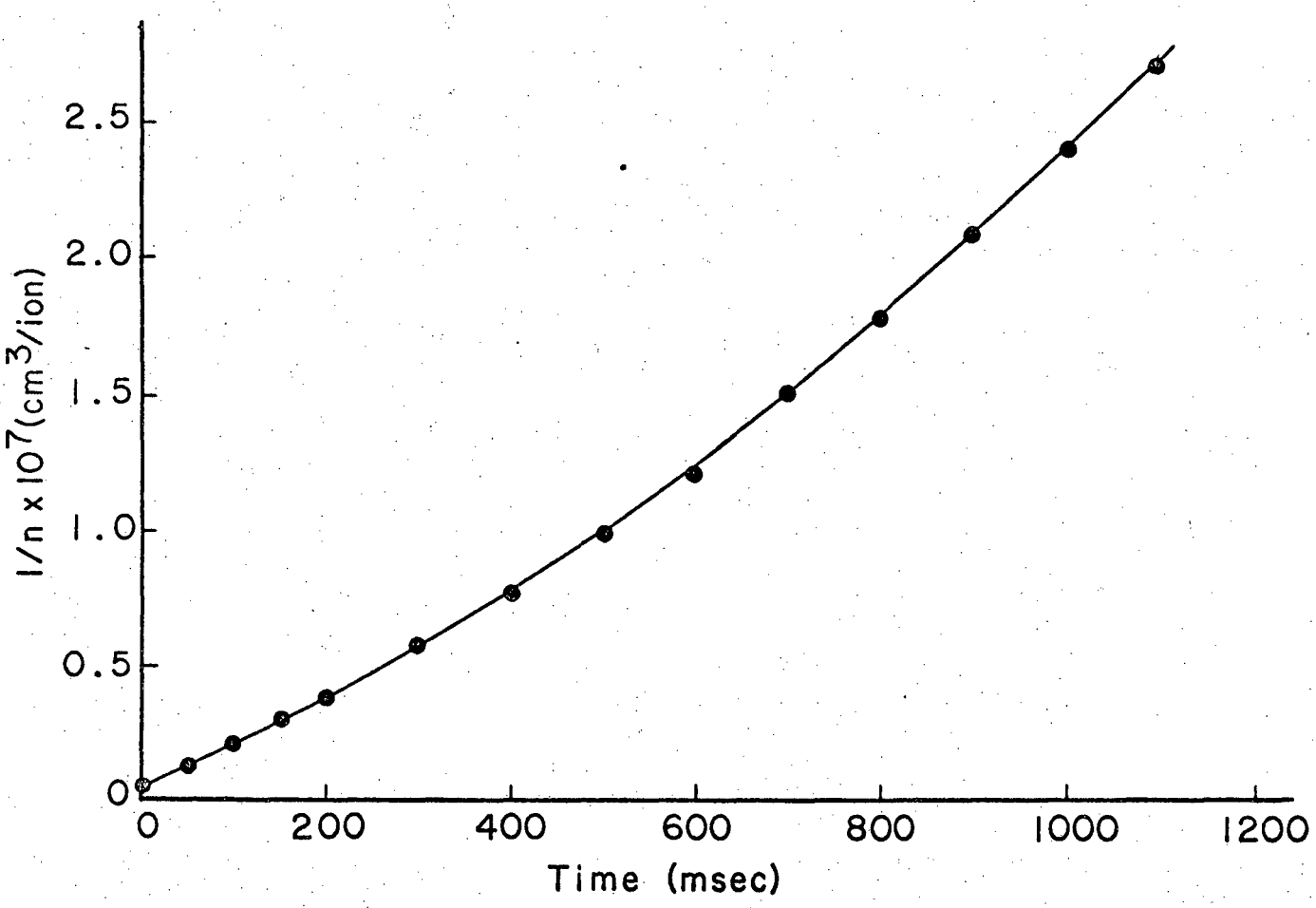

Fig. 6 Plot of 1/n vs time. TlI-Xe at 160 torr. n is the average ion density

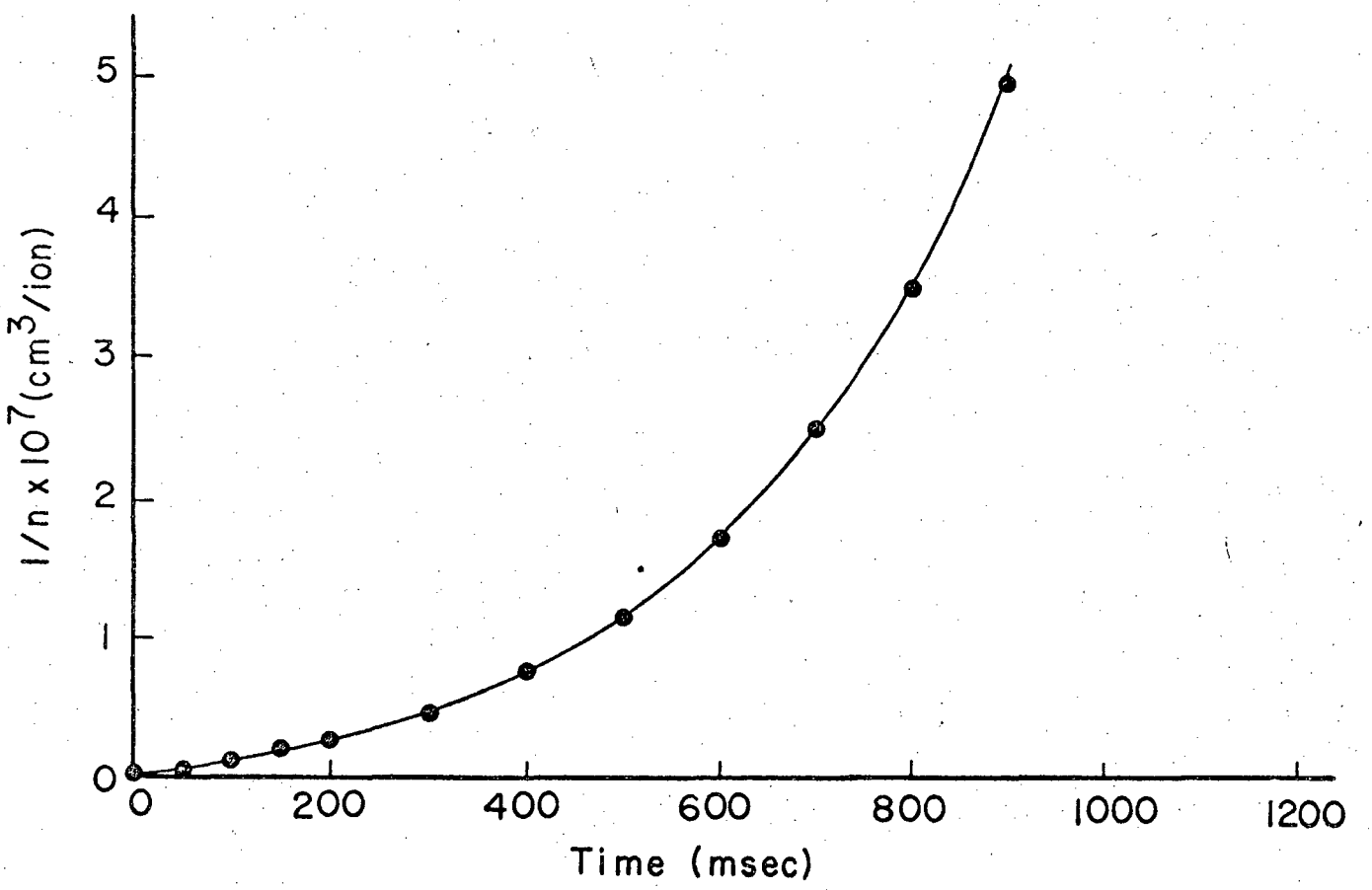

Fig. 7 Plot of 1/n vs time. TlI-Ar at 78 torr. n is the average ion density

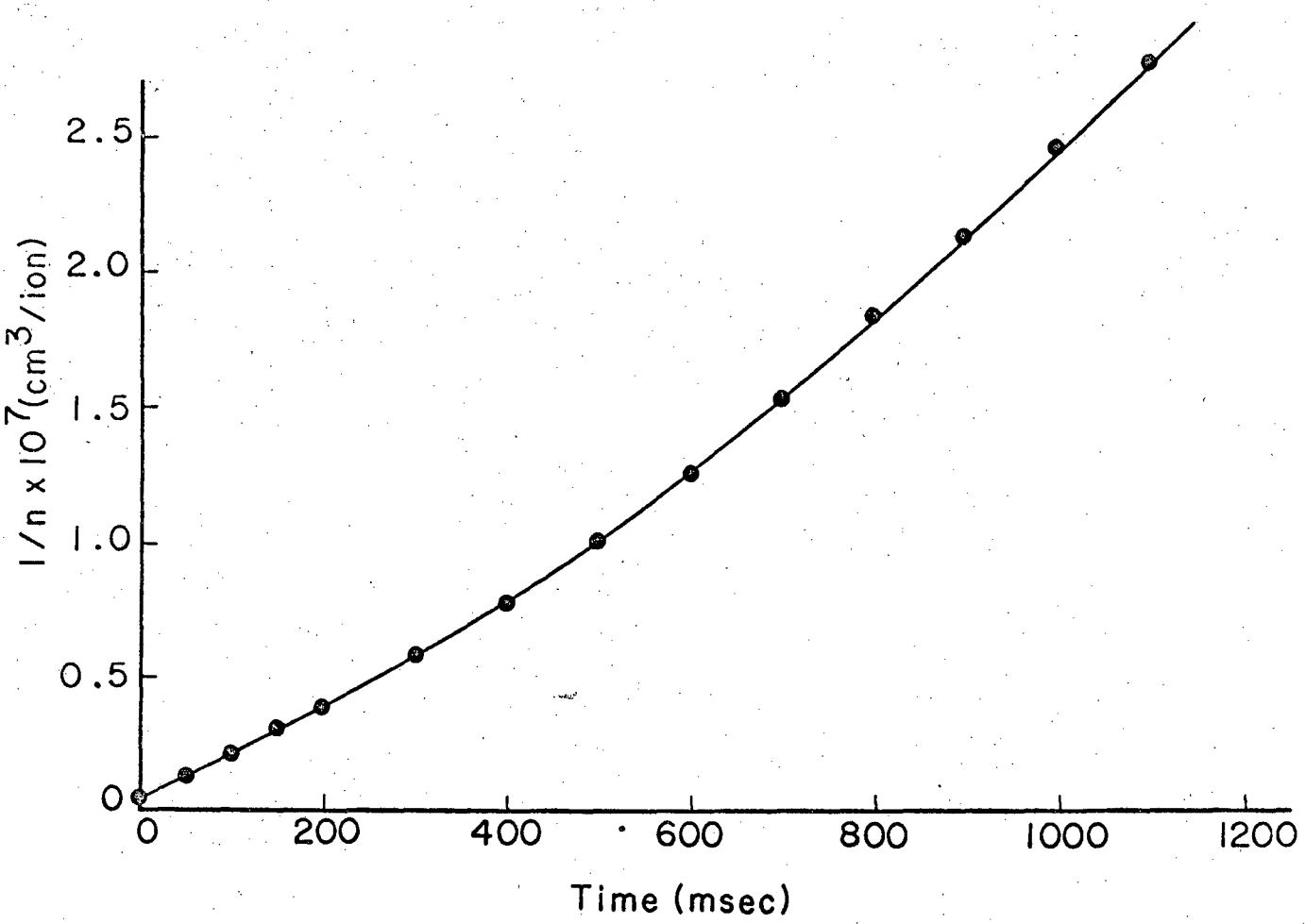

Fig. 8 Plot of 1/n vs time. TlI-Ar at 354 torr. n is the average ion density

Gray and Kerr[1] have given conditions under which diffusion can be neglected in processes involving both recombination and diffusion. They have shown that if the neglect of diffusion is to lead to errors of only a few percent, the plot of 1/n vs t should be linear over a fractional change in 1/n of 8. It is easily seen from Figs. 5-8 that in no case in these experiments can diffusion be neglected. In fact, at the lowest pressures diffusion is the dominant process during much of time observed.

The easiest way to take into account diffusion approximately, is to assume an ion loss equation of the form

$$-\frac{dn}{dt} = \alpha n^2 + \beta n \qquad \text{(III.3)}$$

where β depends only on the geometry of the vessel and not on n. In this equation it is assumed that the diffusion loss can be adequately described by including only the fundamental mode of diffusion.[2] For the geometry in our experiments it is only strictly valid when the ion distribution is cosine. While the quadratic recombination loss term, i.e., αn^2, tends to make the distribution uniform, which invalidates the linear diffusion loss term, the equation can be expected to take into account the main diffusion loss, although its absolute accuracy is difficult to estimate a priori. Equation (III.3) can be easily integrated to give

$$\ln \frac{n[n_o + (\beta/\alpha)]}{n_o[n + (\beta/\alpha)]} = -\beta(t-t_o) \qquad \text{(III.4)}$$

where $n = n_o$ at $t = t_o$. The values of α and β were determined by fitting this equation to 3 points: (n_o, t_o), a point where diffusion is dominant and an intermediate point. An alternate approach is to write Eq. (III.3) as

$$-\frac{d \ln n}{dt} = \alpha n + \beta \qquad \text{(III.5)}$$

and plot ln n vs n. This however requires some numerical or graphical determination of (d ln n)/dt and in view of the scatter in some of the rate curves, the first method proved more convenient.

A more exact analysis given in the next section showed that the results of this method were in fact in error by ~10-20%. This is probably mainly due to the following. At concentrations where diffusion begins to be dominant and the ion density tends to a cosine distribution, the appropriate experimental quantity is determined from Eq. (III.3) averaged over the distribution. Averaging over Eq. (III.3) we obtain with $n = n^o \cos \xi$

$$\frac{dn'}{dt} = \frac{\pi^2}{8} \alpha n'^2 + \beta n' \qquad n' = \frac{\int n dV}{V} \qquad \text{(III.6)}$$

Thus unless the distribution remains substantially uniform in the time interval used, Eq. (III.3) is not an adequate description of the recombination loss.

In view of these results the numerical method described in the next section was used to determine the recombination and diffusion constants.

B. Numerical Determination of Recombination and Diffusion Constants

1. Ambipolar Diffusion

The approximate mass dependence of the mobility and diffusion constants is given by the Langevin[2] equation, in which

$$K, D \propto \frac{1}{\mu^{1/2}} \qquad \text{(III.7)}$$

where K is the mobility, D is the diffusion constant and μ is the reduced mass of the ion and molecule through which the ion is moving. In regions of the plasma where the ion density changes, e.g., near a wall, the ions of the smaller reduced mass or what is the same thing, the ion of the smaller mass diffuses more quickly. This however produces a net charge in the plasma and creates electric fields which retard the motion of the more rapidly moving ions. The net effect is that the two types of ions diffuse as a unit. This is called ambipolar diffusion. A simple calculation[3] of the ambipolar diffusion constant gives

$$D_a = \frac{D^+K^- + D^-K^+}{K^+ + K^-} \qquad \text{(III.8)}$$

and the ion loss is given by the usual equation,

$$\frac{\partial n}{\partial t} = \nabla \cdot (D_a \nabla n) \qquad n = n^+ = n^- \qquad \text{(III.9)}$$

Ambipolar diffusion has been generally applied to the case of electrons and positive ions. In this case the electrons move rapidly to set up the retarding field and ambipolar diffusion appears very quickly. There is no a priori reason not to expect ambipolar diffusion to hold when both ions are massive even in the presence of competitive loss mechanisms, as long as the net charge density remains small compared to the total charge density. Only in cases where electron attachment, charge exchange or such processes are important is it evident that this simple picture is invalid.

It was decided, however, to integrate the exact equations numerically in order to compare the ion loss with that predicted in the ambipolar approximation. We consider the case of a one dimensional cavity whose walls are the infinite plane parallel plates shown in Fig. 9. (While the 4 cm^2 collection electrode is far from infinite, the effect of the guard

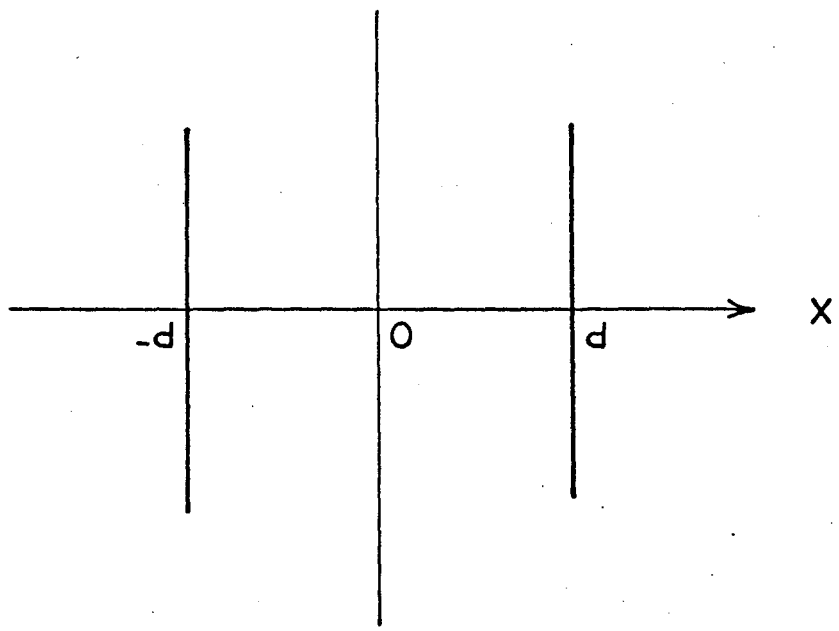

Fig. 9 A one dimensional cavity with plane parallel walls

ring is to make negligible edge effects at the collection electrode.)

The positive and negative current densities are

$$J_+ = -D^+ \frac{\partial n^+}{\partial x} + n^+K^+E$$

$$J_- = -D^- \frac{\partial n^-}{\partial x} - n^-K^-E \qquad \text{(III.10)}$$

Using the equation of continuity

$$\frac{\partial n^\pm}{\partial t} + \frac{\partial J_\pm}{\partial x} + \alpha n^+n^- = 0 \qquad \text{(III.11)}$$

we obtain

$$\frac{\partial n^+}{\partial t} = D^+ \frac{\partial^2 n^+}{\partial x^2} - K^+ \frac{\partial(n^+E)}{\partial x} - \alpha n^+n^- \qquad \text{(III.12)}$$

and

$$\frac{\partial n^-}{\partial t} = D^- \frac{\partial^2 n^-}{\partial x^2} + K^- \frac{\partial(n^-E)}{\partial x} - \alpha n^+n^- \,. \qquad \text{(III.13)}$$

Poisson's equation is

$$\frac{\partial E}{\partial x} = 4\pi e(n^+ - n^-) \qquad e > 0 \qquad \text{(III.14)}$$

and the boundary equations are

$$n^\pm(-d,t) = n^\pm(d,t) = 0 \,. \qquad \text{(III.15)}$$

Since the density is symmetrical about the origin

$$E(x) = -E(-x) \,. \qquad \text{(III.16)}$$

In terms of the following reduced parameters

$$P^+ = \frac{n^+}{n_o}, \quad P^- = \frac{n^-}{n_o}, \quad \xi = \frac{x}{d}, \quad \tau = \frac{D^+}{d^2}t, \quad U = \frac{Ed}{kT} \qquad \text{(III.17)}$$

and using

$$K^{\pm} = \frac{e}{kT} D^{\pm} \tag{III.18}$$

Equations (LLL.12 - III.16) become

$$\frac{\partial P^+}{\partial \tau} = \frac{\partial^2 P^+}{\partial \xi^2} - \frac{\partial (P^+ U)}{\partial \xi} - \Omega P^+ P^- \tag{III.19}$$

$$\frac{\partial P^-}{\partial \tau} = R \frac{\partial^2 P^-}{\partial \xi^2} + R \frac{\partial (P^- U)}{\partial \xi} - \Omega P^+ P^- \tag{III.20}$$

$$\frac{\partial U}{\partial \xi} = G(P^+ - P^-) \tag{III.21}$$

$$U(\xi) = -U(\xi) \tag{III.22}$$

$$P^{\pm}(-1,\tau) = 0 \tag{III.23}$$

$$P^{\pm}(1,\tau) = 0$$

where

$$\Omega = \frac{\alpha n_o d^2}{D^+}$$

$$R = D^-/D^+ \tag{III.24}$$

$$G = \frac{e^2 d^2}{kT} \; 4\pi n_o$$

In order to solve these equations on the SDS 610 computer they were replaced by the following difference equations

$$P^+(\xi_i,\tau_{j+1}) = P^+(\xi_i,\tau_j) + \Delta\tau \left\{ \frac{[\delta^2 P^+]_i^j}{(\Delta\xi)^2} - \frac{[\delta(P^+U)]_i^j}{2\Delta\xi} - \Omega P^+(\xi_i,\tau_j) P^-(\xi_i,\tau_j) \right\} \tag{III.25}$$

$$P^-(\xi_i,\tau_{j+1}) = P^-(\xi_i,\tau_j) + \Delta\tau\left\{R\frac{[\delta^2P^-]_i^j}{(\Delta\xi)^2} + R\frac{[\delta(P^-U]_i^j}{2\Delta\xi} - \Omega P^+(\xi_i,\tau_j)P^-(\xi_i,\tau_j)\right\} \tag{III.26}$$

where

$$P^{\pm}(\xi_i,\tau_j) = P^{\pm}(i\Delta\xi, j\Delta\tau)$$

$$[\delta^2P^{\pm}]_i^j = P^{\pm}(\xi_{i+1},\tau_j) - 2P^{\pm}(\xi_i,\tau_j) + P^{\pm}(\xi_{i-1},\tau_j) \tag{III.27}$$

$$[\delta(P^{\pm}U)]_i^j = P^{\pm}(\xi_{i+1},\tau_j)\,U(\xi_{i+1},\tau_j) - P^{\pm}(\xi_{i-1},\tau_j)\,U(\xi_{i-1},\tau_j)$$

The solution proceeded as follows: At $\tau = 0$, $U = 0$ and from the initially assumed distribution, $P^{\pm}$ were calculated from the difference equations at $\tau = \Delta\tau$. Due to the difference in diffusion constants, i.e., $R \neq 1$, a net charge density was formed. Equation (III.21) was then integrated to give values of U and Eqs. (III.25) and (III.26) were applied again with the new values of P and U to give $P^{\pm}$ at $\tau = 2\Delta\tau$. The process is then repeated. At various time intervals the charge densities were integrated to give the total positive and negative charge remaining.

The following case was solved and the results are found in the first three columns of Table I; Tl^+, I^- in Xe at 95.5 torr, 532°K. The density was assumed uniform except for a cosine fall off near the walls and the volume chosen was 7 cm^3. The concentrations given are the total ions remaining divided by the volume. The recombination constant α is 9.0×10^{-8} and the diffusion constants were calculated from Langevin's equation using Eq. (III.29) of Section 2.

The rate loss assuming ambipolar diffusion is found by solving the equation

$$\frac{\partial n}{\partial t} = D_a \frac{\partial^2 n}{\partial x^2} - \alpha n^2 \qquad \text{(III.28)}$$

where D_a is given by Eq. (III.8). This equation was solved using difference equations similar to those just described and the results are given in column four of Table I. The last column gives the ion loss without diffusion in order to show the magnitude of the diffusion correction.

Table I. Comparison of exact ion loss rate with that obtained assuming ambipolar diffusion. Average ion concentrations are given.

time (msec)	exact ion conc. ion/cc 10^{-8} positive	negative	ion conc. with ambipolar diffusion	ion conc. without diffusion
0	2.679	2.679	2.679	2.679
50	1.039	1.038	1.038	1.216
100	.6183	.6177	.6180	.8853
150	.4283	.4279	.4281	.5803
200	.3211	.3208	.3209	.4601
250	.2527	.2524	.2525	.3812
300	.2055	.2052	.2053	.3254
350	.1711	.1708	.1709	.2838
400	.1450	.1447	.1448	.2517
450	.1245	.1243	.1244	.2261
500	.1082	.1079	.1081	.2052
550	.09476	.09453	.09465	.1879
600	.08363	.08341	.08353	.1732
650	.07425	.7405	.07416	.1607
700	.06628	.06608	.06619	.1499
750	.05942	.05923	.05930	.1404
800	.05348	.05329	.05340	.1320
850	.04830	.04812	.04821	.1246
900	.04373	.04356	.04366	.1180
950	.03971	.03954	.03962	.1120

It can be seen from the table that ambipolar diffusion is very accurately obeyed in the density range studied. Since it was in this range that the experiments were done Eq. (III.28) was adapted to analyse the experimental rate curves. The transition from ambipolar to free diffusion will invariably occur when the charge density becomes sufficiently small. Allis and Rose[4] have analyzed the transition region for electron ion diffusion and obtained an effective diffusion constant in the transition region.

2. Experimental Diffusion Constants and Recombination Coefficients

In the limit where only ion-molecule polarization forces are important the Langevin theory[2] gives for the mobility the equation

$$K = \frac{0.5105}{[4\pi\alpha]^{1/2}} \frac{1}{N} \frac{1}{\mu^{1/2}} \qquad \mu = \frac{Mm}{M+m} \qquad \text{(III.29)}$$

where M is the mass of the molecule, m the mass of the ion, α the polarizability of the molecule, and N the molecule number density.

It was found that the diffusion constants calculated from Eq. (III.29) were in every case larger than those obtained from experimental results. It was found however that a linear dependence on temperature and inverse dependence on density was valid. Thus we can write

$$D_a = C \frac{T}{N} \qquad \text{(III.30)}$$

where C is independent of T and N.

Equation (III.28), which has two unknown parameters, D_a and α, was fit to the experimental curve by trial and error. The value of D_a and thus C [in Eq. (III.30)] were determined from the low pressure experiments where diffusion is dominant. It was found that experiments at other

pressures could be fit reasonable well in accordance with Eq. (III.30). Deviations were random.

The last column in Table X of Chapter IV presents the values of C determined from experiment. The other data presented there are predictions from the Langevin theory and are discussed in Chapter IV.

Tables II and III present the recombination coefficients at the various pressures studied. The error limits are estimated from the numerical fit to the experimental points. A "perfect" fit to a smooth set of points would give an uncertainty in α of about $\pm .1\times10^{-8}$ as being graphically meaningful. The main errors in fitting the curves arose from the fact that a given value of C determined from low pressure curves was not the "best" value for all pressures. Most curves could have been fit better by determining the "best diffusion" constant but this only places all the errors in the fluctuation of the diffusion constant and none in the fluctuations in α. When a value of C was chosen more importance was placed in fitting the curve at small times when recombination is most important than in the diffusion dominated regions. The smooth curves in Figs. 5-8 are the numerical fits determined by the above method.

A temperature correction was applied to several of the thallium bromide points in order that the plot of α vs pressure refers to a single temperature. The correction was made using Eq. (III.32) of the next section where the values of C_1 and C_2 were estimated from the α vs pressure plots. The plots of α vs pressure are given in Figs. 10-13.

Table II. Recombination Coefficient α. (Xe)

Pressure (torr)	Temperature (°K)	$\alpha \times 10^8$ (cm^3/sec)	Pressure (torr)	Temperature (°K)	$\alpha \times 10^8$ (cm^3/sec)
TlI - Xe			TlCl - Xe		
34	533	6.5±.4	48.5	620	7.0±.4
47	530	6.5±.4	56	613	7.0±.5
71	533	8.0±.5	68	613	7.3±.5
95.5	532	9.5±.4	99.5	621	8.5±.6
117.5	533	10.0±.5	150	622	10.0±.5
144	523	12.0±.6	156	616	10.0±.5
160	531	12.5±.5	191	610	10.6±.4
190	513	14.5±.7	237	612	11.0±.6
240	530	18.0±.8	279	603	12.5±.7
TlBr - Xe			TlI-NO_2 - Xe		
38	593	6.5±.3	42	554	6.5±.3
74	593	7.2±.3	49	555	6.75±.4
98.5	596	8.3±.4	72	555	7.75±.5
126	593	9.0±.3	73	553	7.8±.4
136.5	596	9.5±.3	76	548	7.25±.5
178	547	[b]11.5±.7	99	555	8.75±.6
222	547	[b]13.5±.7	110	553	8.0±.5
			150	555	9.4±.5
			152	553	10.2±.6
			152.5	548	10.0±.6
			186	558	10.5±.5
			198	556	10.5±.5

b. A temperature correction was applied in plotting this point.

Table III. Recombination Coefficient α (Ar)

Pressure (torr)	Temperature (°K)	$\alpha \times 10^8$ (cm^3/sec)	Pressure (torr)	Temperature (°K)	$\alpha \times 10^8$ (cm^3/sec)
	TiI - Ar			TlCl - Ar	
78	530	6.0±.3	210	608	9.5±.5
139.5	531	7.3±.4	300	619	9.75±.5
193	531	9.5±.6	304	606	11.0±.7
269	531	10.5±.6	354.5	608	11.0±.6
354	528	12.4±.4	432	610	12.5±.5
	TlBr - Ar			$TlI-NO_2$ - Ar	
54.5	591	5.5±.4	55.5	547	6.0±.4
107	591	7.3±.5	104	555	6.75±.4
147	561	[b]8.0±.7	150	548	7.3±.4
186	591	9.0±.6	199	554	7.7±.4
226	561	[b]9.0±.7	296.5	548	9.2±.5
308	561	[b]10.0±.5			
394	561	[b]11.5±.8			

b. A temperature correction was applied in plotting this point.

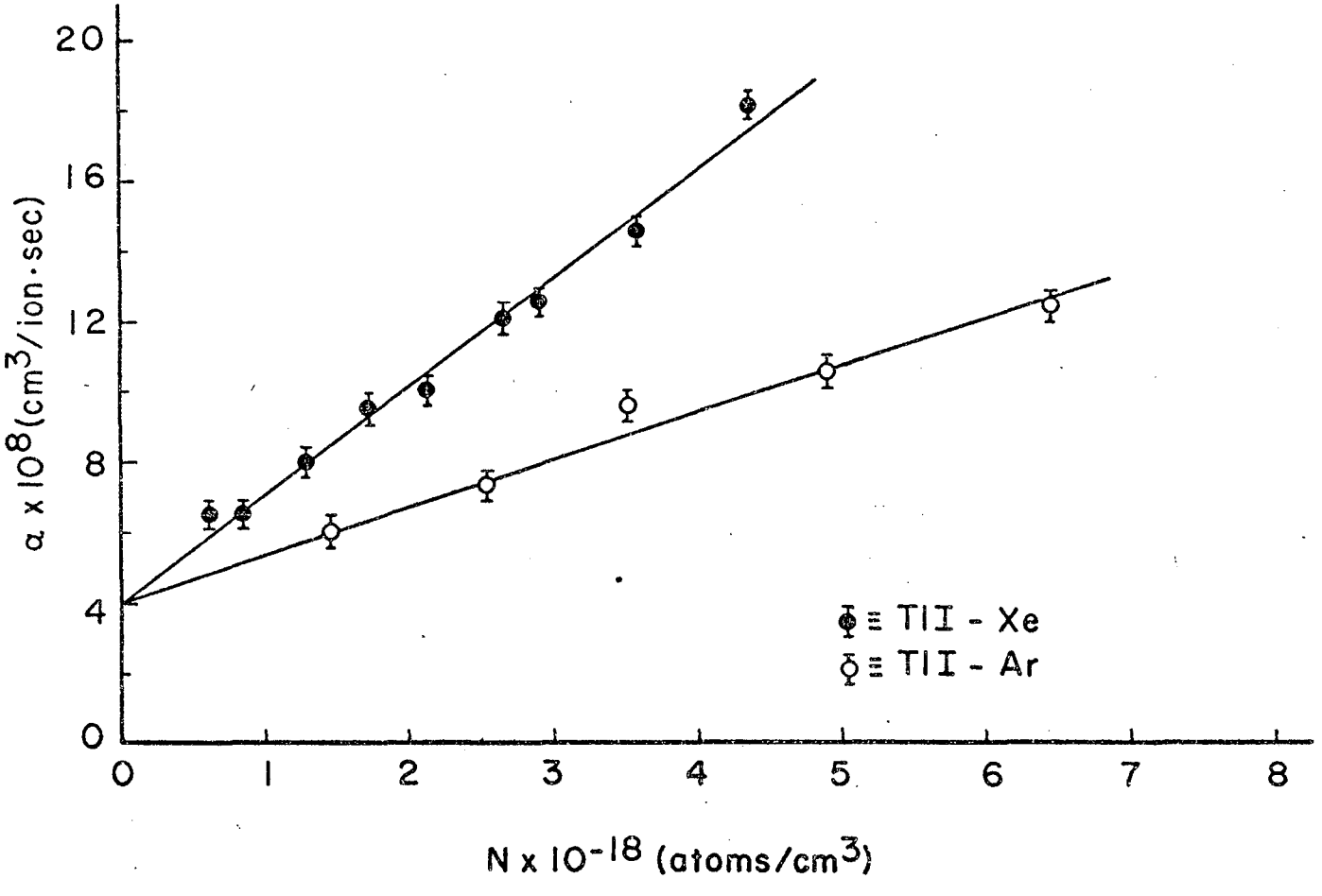

Fig. 10 Plot of recombination coefficient vs no. density for TlI

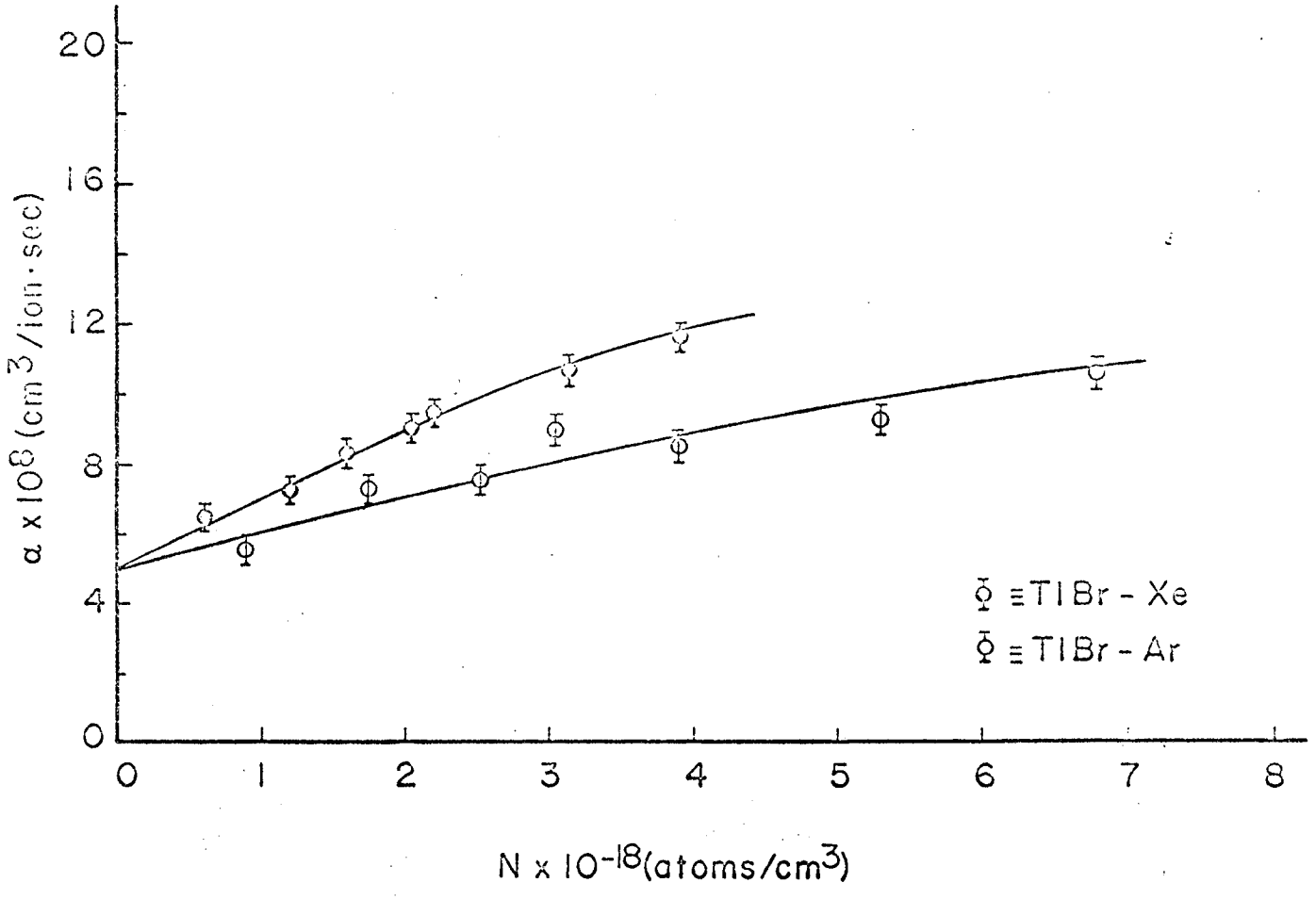

Fig. 11 Plot of recombination coefficient vs no. density of TlBr

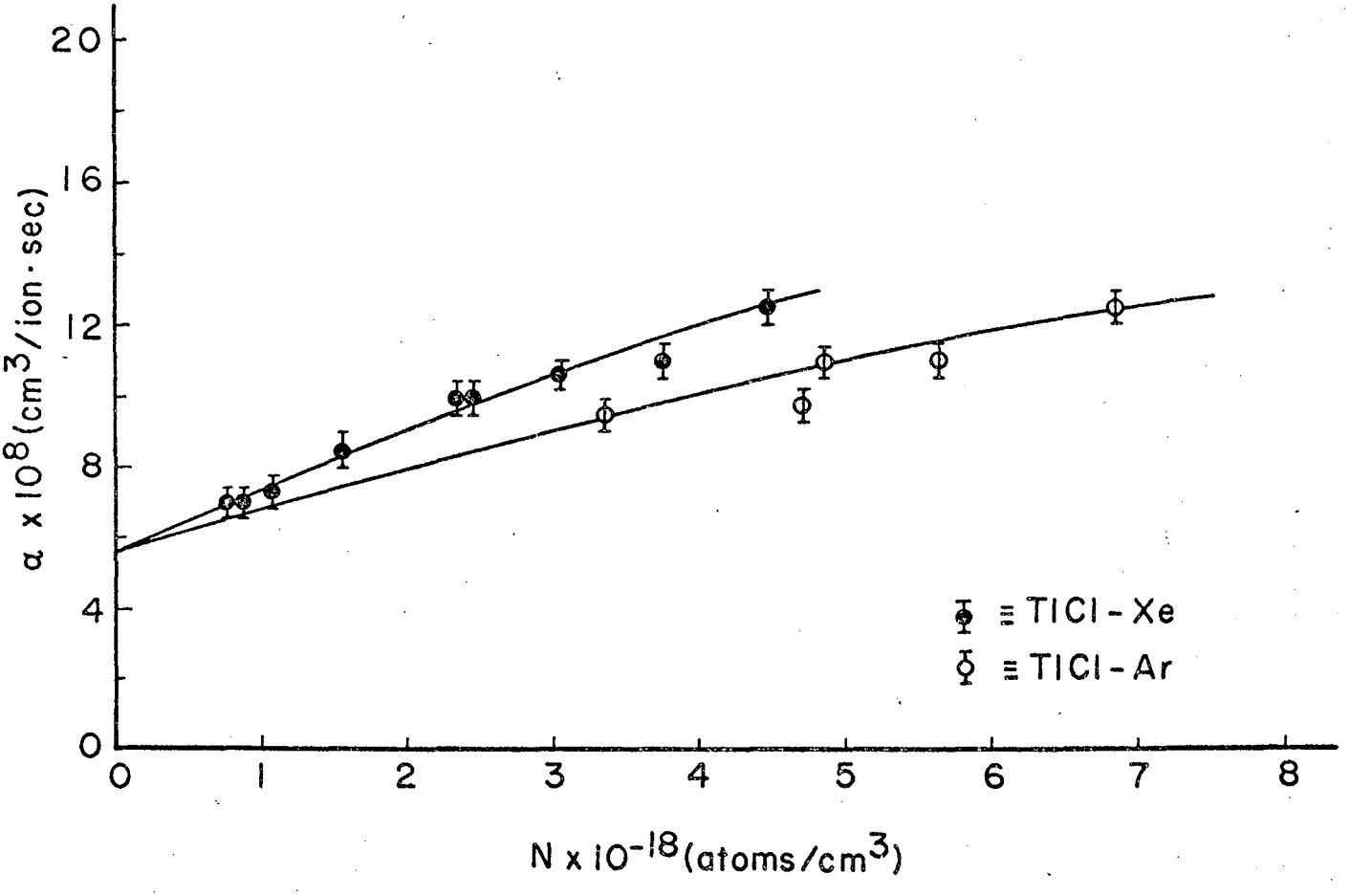

Fig. 12 Plot of recombination coefficient vs no. density for TlCl

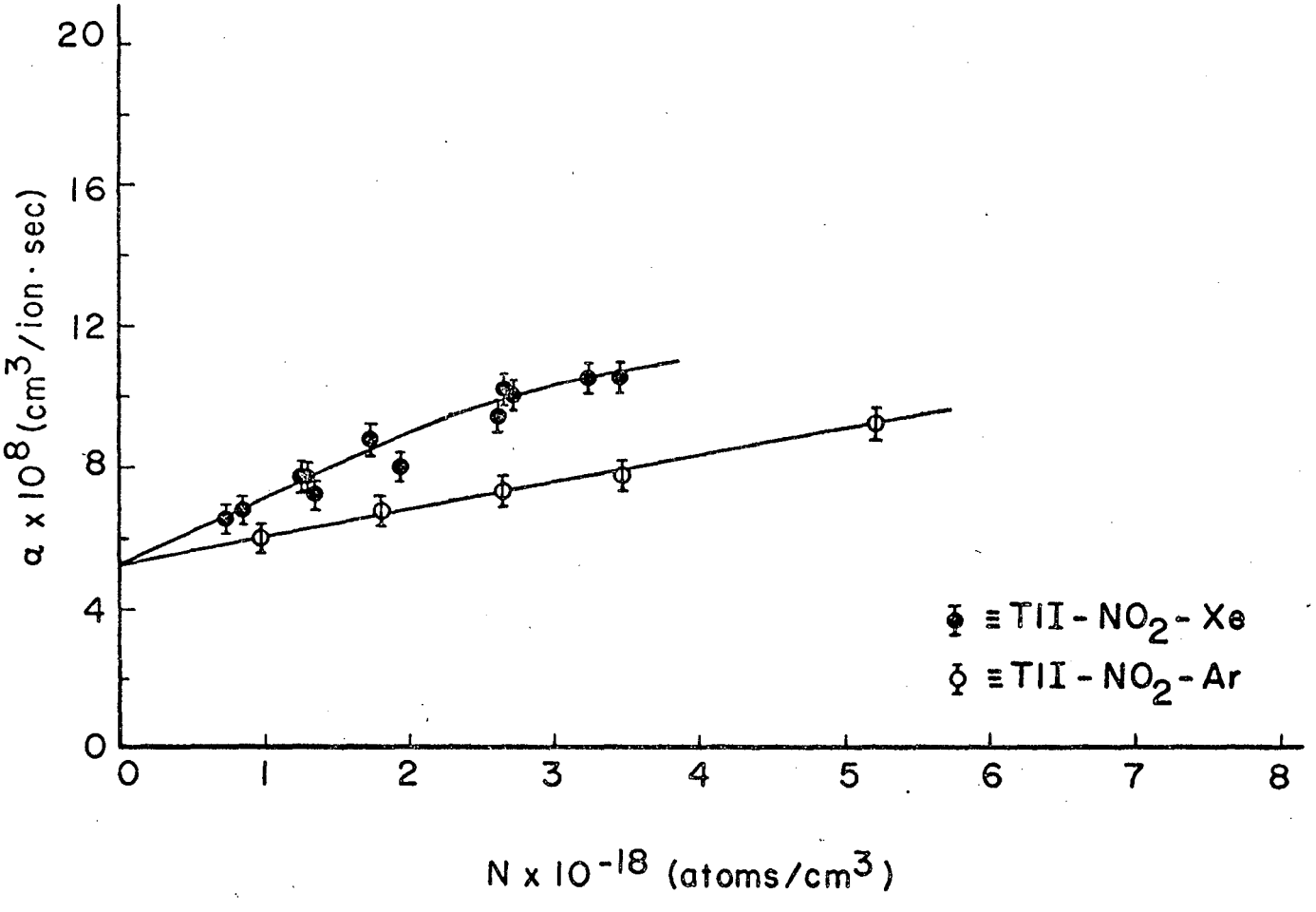

Fig. 13 Plot of recombination coefficient vs NO_2 density for $TlI-NO_2$

C. Temperature Dependence of the Recombination Coefficient

An attempt was made to measure the temperature dependence of the rate at constant pressure in the case of thallium iodide in xenon. This case allowed the widest range of possible temperatures since TlI could be done at a lower temperature than the other halides. The main difficulty in these measurements is the rather small range of temperatures which can be studied; intensity requirements allowed only a 20% variation in the temperature. The pressure was chosen with regard to minimizing errors due to diffusion on the one hand and finite ion collection times on the other. The recombination coefficients at the various temperatures are given in Table IV and the results plotted in Fig. 14.

The temperature dependence of the rate is divided into two terms; the two body pressure independent term (the zero pressure extrapolation) and the three body rate which at low pressure is linear in the third body density. Thus at low pressures we can write

$$\alpha = \alpha_o + \alpha_3 N \qquad \text{(III.31)}$$

where α_o and α_3 are independent of N. From the results of Chapter V we can determine the temperature dependence of these two factors. α_o is probably accurately proportional to the inverse square root of the temperature and α_3 is approximately proportional to T^{-3}. Thus we can write approximately

$$\alpha = C_1 T^{-1/2} + C_2 T^{-4} P \qquad \text{(III.32)}$$

where P is the pressure and C_1 and C_2 are independent of T. Using for α_o the value obtained from Fig. 10, (4.0×10^{-8} $cm^3 sec.^{-1}$) the smooth

Table IV

Recombination Coefficient α(Temperature Dependence)

Pressure (torr)	Temperature (°K)	$\alpha \times 10^8$ (cm^3/ion · sec)
177	493	14.5±.5
176	499	14.0±.5
177	531	14.0±.6[a]
177	545	13.25±.5
177.5	571	11.5±.5
177	605	9.5±.7
176.5	610	11.0±.7

a. This point was taken from Fig. 10.

curve in Fig. 14 corresponds to the equation

$$\alpha = 4.0\times10^{-8} \left(\frac{531}{T}\right)^{1/2} + 9.25\times10^{-8} \left(\frac{531}{T}\right)^{4} \qquad \text{(III.33)}$$

The lack of accurate data over a wide range of temperatures makes it difficult to draw any conclusions concerning the temperature dependence of the rate. The scatter is appreciable especially in the upper and lower temperature limits. These limits might be extended considerably on the high temperature side, and by the use of reflecting mirrors and higher voltage sparks, which would increase the ionization radiation, it might be extended 10-20 degrees on the low temperature side. Thorough study of this extended range should give valuable information on the two and three-body temperature dependence. All that can be said in the present study is that there is no obvious conflict with the experiment and present theory.

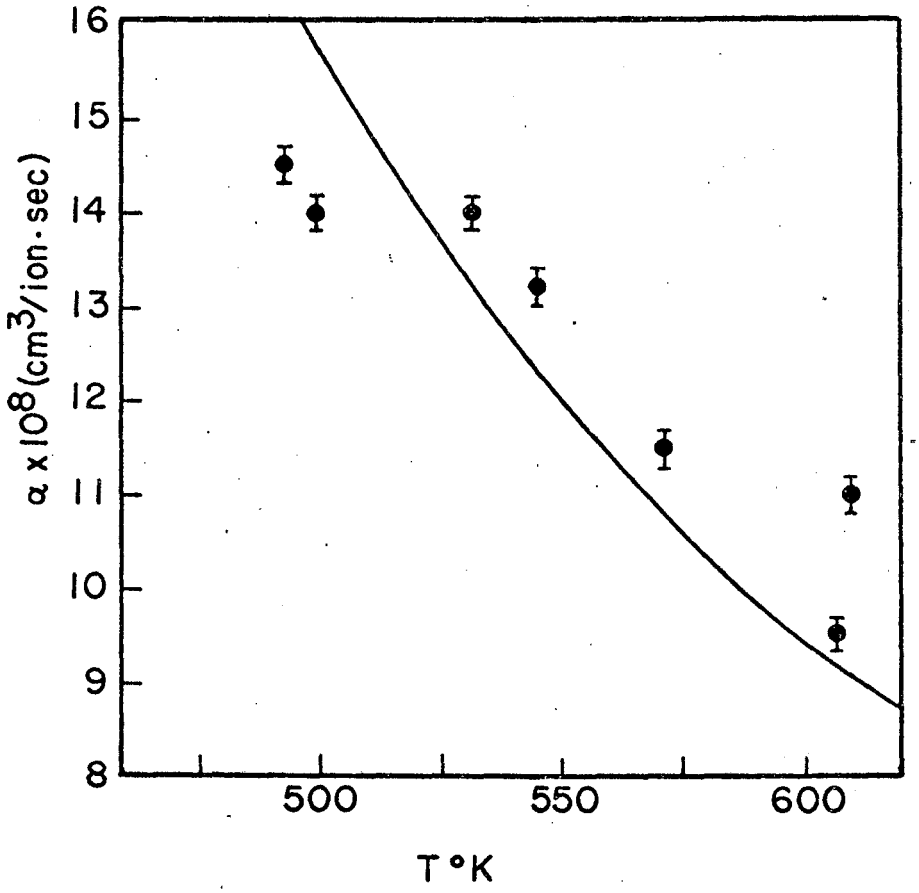

Fig. 14 Temperature dependence of the recombination coefficient at constant pressure

References for Chapter III

1. E. P. Gray and D. E. Kerr, Ann. Phys. (New York) 17, 276 (1962).

2. E. W. McDaniel, Collision Phenomena in Ionized Gases (John Wiley and Sons, New York, 1964) Chap. IX and X.

3. E. W. McDaniel, Collision Phenomena in Ionized Gases (John Wiley and Sons, New York, 1964) p. 513.

4. W. P. Allis and D. J. Rose, Phys. Rev. 93, 84 (1954).

IV. NATURE OF THE IONIZED GAS

This chapter is devoted to the study of the extent to which atomic ions form complexes with the parent molecules or inert background gas.

The primary photochemical process has been shown to be[1]

$$TlX + h\nu \longrightarrow Tl^{+} + X^{-} \qquad (IV.1)$$

If the primary ions are not formed with sufficient kinetic energy, collisions with the inert gas will tend to reform the initial molecule. The collision frequency at 100 torr is $\sim 10^{8}$/sec. Thus an ion will undergo $\sim 10^{5}$ collisions with the inert gas before the first concentration measurement is made, 2 milliseconds after the ions are formed. Feibelman[2] has shown that the stability of ion pairs is decided in the first few collisions. Thus if there is tendency to form correlated ion pairs in the initial photochemical process, the effect of such pairs is determined very quickly; either the ions recombine to form the initial molecule or they get lost in the body of the gas. Consequently no effects due to correlated ion pairs are expected and none were observed.

A. Mass Spectrometry

An attempt was made to determine directly the ionic species present when the thallium halides are photolyzed in the presence of an inert background gas. Terenin and Popov[2] determined with a crude mass spectrometer that the atomic ions are produced upon photolyzing thallium iodide and thallium bromide in the absence of a background gas. Although the sensitivity was low their experiments did not indicate the presence of species other than the atomic ions.

Results are obtained here for thallium iodide. The other halides are less photo-sensitive and a strong continuous source of ionizing

radiation was not available for them.

1. Mass Spectrometer

A radio frequency mass spectrometer built by Dr. Yuan-Tseh Lee was used in the analysis. It was adapted from an apparatus described by Boyd and Morris,[3] and is essentially a small 12-stage linear accelerator designed to accelerate preferentially ions of a given mass to charge ratio. It will operate at pressures up to 1 torr and higher depending on the size of the sampling orifice and the speed at which the gas is pumped. Figure 15 gives a schematic diagram of the spectrometer.

A source of ionizing radiation produces ions between electrodes A and B. A small potential between A and B draws ions of the appropriate sign through the sampling orifice and they are accelerated through a large voltage (V_a) between B and C. (Although the spectrometer is designed to operate at an accelerating voltage between 500-1000 volts, smaller voltages were necessary in these experiments to prevent discharging in the background gas.) The energy imparted by the accelerating voltage is large compared to the energy of the ions entering the orifice and so gives rise to a velocity distribution $v = (2V_a e/m)^{1/2}$ depending on the e/m ratio for the ions and not significantly on their initial velocity. The accelerating electrode C is maintained at ground potential in order that the radio frequency signal (5 volts) applied to the electrodes E may be relative to ground. The electrodes F and the screen which surrounds the radio frequency electrodes are also maintained at ground potential. The energy gained by the ions depends on both the magnitude and frequency of the radio frequency signal and on the e/m ratio of the ions. The radio frequency signal is large enough that the energy gain is sufficient to make mass discrimination possible although

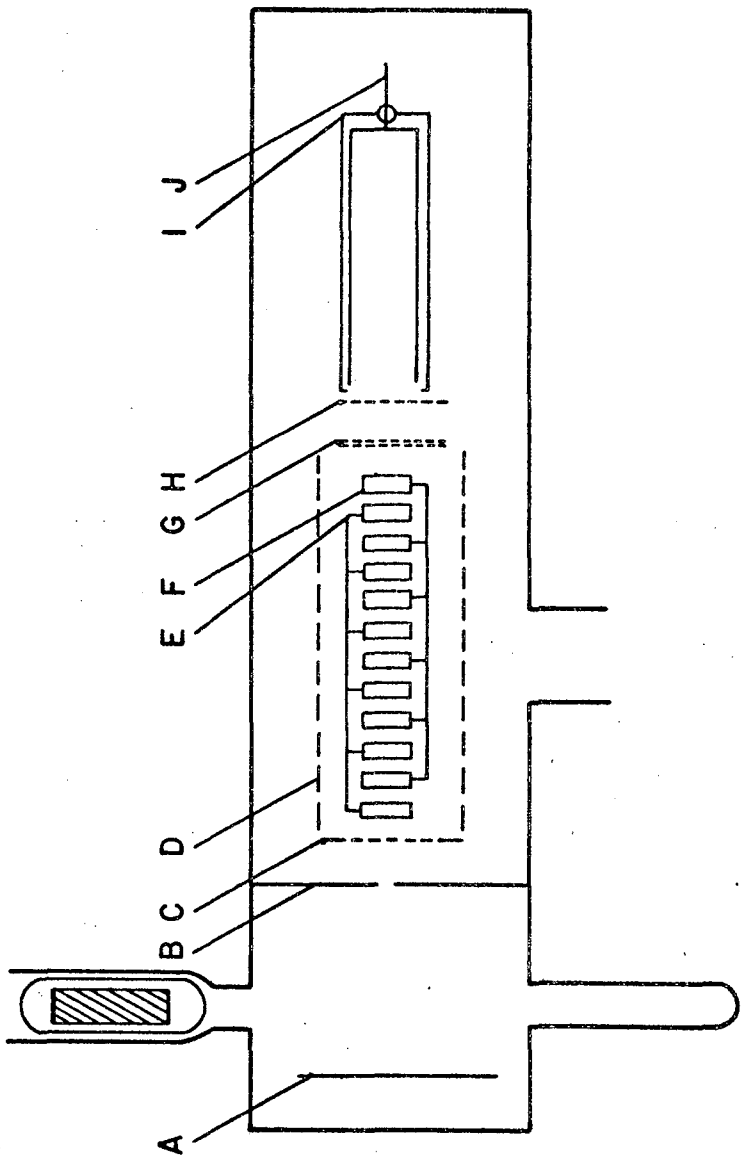

Fig. 15 Schematic diagram of the mass spectrometer

the time of flight through the electrode region is not appreciably changed. The frequency corresponding to the maximum energy gained for singly charged ions and .5 cm radio frequency electrode spacing is given by[3]

$$f^2 = V_a \frac{5.70\times10^{14}}{M} \ (\mathrm{sec}^{-2}) \qquad \text{(IV.2)}$$

where V_a is the accelerating voltage and M is the molecular weight of the ion. In addition there are subsidiary peaks of smaller intensity on either side of the maximum.

If the potential of the retarder grid G is set[3] 2.57 V_m volts (V_m is the radio frequency voltage) in excess of the accelerating voltage only ions corresponding to the above maximum have sufficient energy to pass the grid G. The electrode H is maintained at an accelerating potential in order to reject all ions of the opposite sign to those in the beam. The shield I around the collection cup J is maintained at ground potential. It should be mentioned that the operation described above differs from that of Boyd and Morris in one respect. In their spectrometer the radio frequency electrodes were connected to a symmetrical oscillator rather than grounding one set of the electrodes. This, however, only affects the first and last electrode and the analysis[3] leading to Eq. (IV.2) is changed little.

The spectrometer is mounted in a quartz tube, the sampling region between electrodes A and B being fitted with optical quartz windows to allow the UV ionizing radiation to enter. The electrodes C and F and the shields D and I are grounded together and all electrodes are spot-welded to kovar leads which pass to the outside through kovar to glass seals.

In order to insure good differential pumping the sampling region

must be well isolated from the rest of the spectrometer. Isolation is accomplished at the electrode B. This electrode was fused into a vacuum tight sandwich between two highly polished quartz discs. This sandwich was then fused to the wall of the main quartz tube. A construction diagram of the spectrometer is given in Fig. 16.

A copper envelope (see Fig. 16) fits around the quartz tube in the region of the radio frequency electrodes and passes around the vacuum connection and into a liquid nitrogen trap to increase pumping efficiency. The entire apparatus is enclosed in a transite oven which allows heating of the sampling region. A magnetically actuated ground glass seal prevents the vapor from condensing outside the heated region. The sample whose vapor is to be studied is placed in a tube extending from the base of the sampling region and into a separately heated oven.

The signal from a Hewlett Packard test oscillator was amplified to provide the radio frequency voltage and a Cary vibrating reed electrometer was used to measure the ion current.

2. Light Source

The maximum in the thallium iodide photosensitivity curve lies at 2125 Å[1] and falls off gradually towards shorter wavelengths. An iodine lamp described by Harteck, Reeves, and Thompson[4] has a strong iodine emission line at 2062 Å. It corresponds to a transition between the $6s^2P_{3/2}$ level and the $5p^5\ ^2P_{1/2}$ rather than the ground state $5p^5\ ^2P_{3/2}$ and thus is not a resonance line.

The lamp used in the mass spectrometer experiments was a discharge excited by the $\simeq$ 3000 Mc microwaves produced by a QK-62 magnetron operating at a power input of 100-150 watts. Lamps were made at various pressure of Ar used as a buffer gas and it was found that a lamp filled

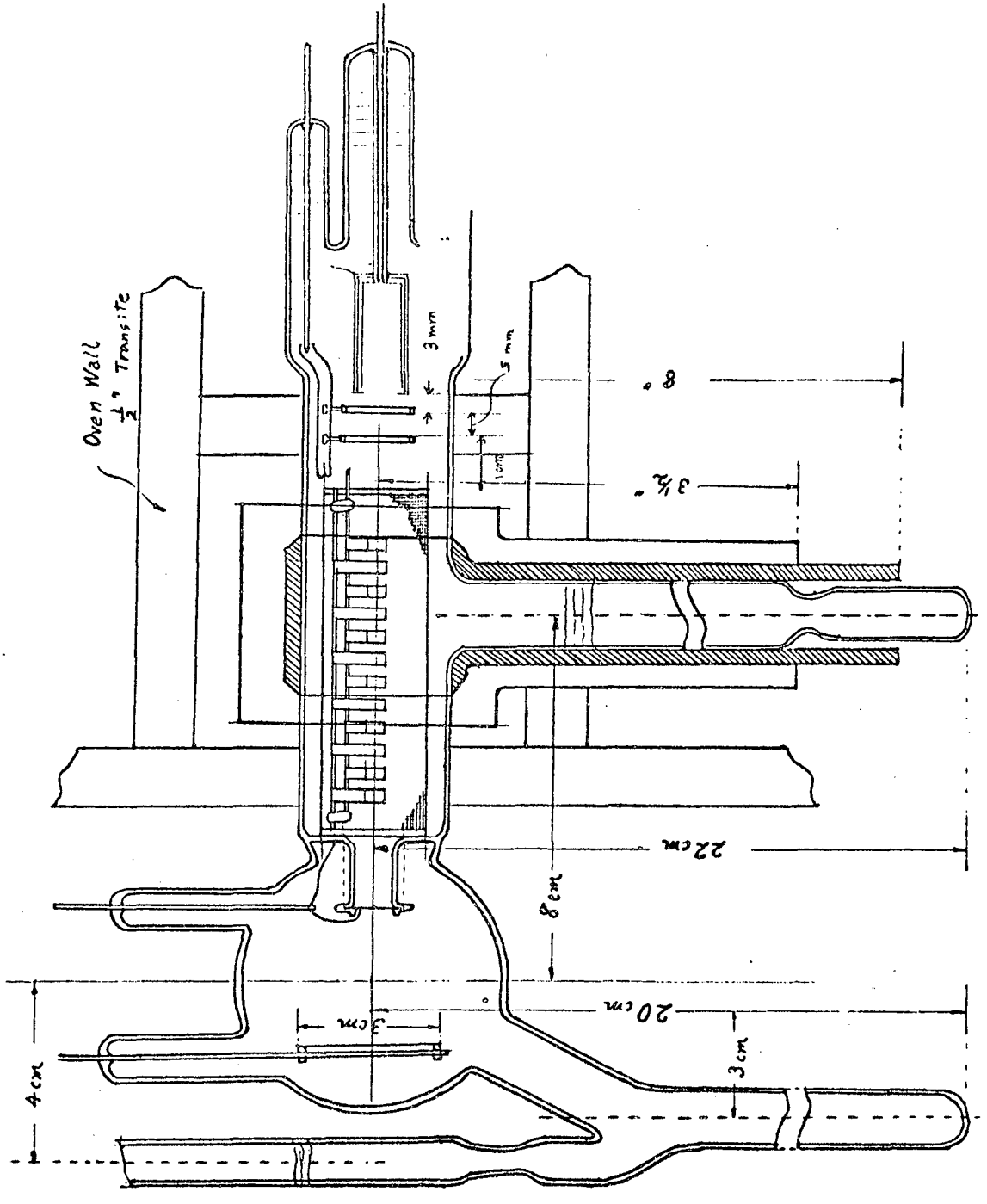

Fig. 16 Construction diagram of the spectrometer

with a small amount of pure iodine operating at room temperature with no buffer gas produced the most intense radiation at 2062 Å. Considerable care had to be taken to insure that the quartz lamp was free from water otherwise the intensity was poor.

A quartz tube fitted with a suprasil quartz window was heated in air until surface impurities were burned off. A small amount of iodine was heated under vacuum to remove water and a small quantity was then distilled into the lamp which was then sealed off.

3. Results

It was found that the spectrometer gave considerably more signal at lower accelerating voltages (V_a) than the specified 500-1000 volts. When nitrogen dioxide was added to study the ions present in the corresponding recombination experiments, discharging occurred with $V_a \gtrsim 375$ volts. In the experiments reported here $V_a = 357$ volts. Equation (IV.2) then becomes

$$f^2 = \frac{6.78}{M} \times 10^{14} (1/\text{sec})^2 \qquad \text{(IV.3)}$$

Because of the low accelerating voltage the effect of the radio frequency signal on the time of flight through the spectrometer, although ignored in deriving Eq. (IV.2), is not completely negligible. While a smaller radio frequency signal reduced the effect, it also reduced somewhat the signal intensity. The small (0-5 volt) voltage between electrodes A and B also increased the effective velocity through the radio frequency region. The result of an effective higher velocity is an apparent lighter mass and correspondingly higher frequency. The observed peaks were generally a few percent higher in frequency than the values predicted by Eq. (IV.3). Further complexing would have the opposite effect, so the error is definitely an instrumental one.

The first group of experiments was done at ~ 630°K where the thallium iodide vapor pressure is ~ 40μ. An attempt was made to use xenon as an inert background gas in the ionizing chamber at a pressure of one torr. It was found however that the pumping speed for xenon of the cooled walls in the accelerator region of the spectrometer was inadequate to prevent destruction of the ion beam through scattering. Sulfur hexafluoride on the other hand had a sufficiently lower vapor pressure at the wall temperature that adequate signal was obtained and it was consequently used as a background gas. The pressure of sulfur hexafluoride in the experiments was one torr. In experiments with nitrogen dioxide the NO_2 pressure was about 70μ. The experimental results are given in Table V. The second group of experiments was done at ~ 720°K where the thallium iodide vapor pressure is approximately one torr. These results are given in Table VI. In Tables V and VI the number in parenthesis to the right of the experimental peak is the frequency predicted by Eq. (IV.3) for the ion indicated below. The bracketed numbers are relative intensities and only have significance in a given column.

Although a slow drift of $\sim 10^{-15}$ amps/sec was present, peaks of 2×10^{-15} amps could easily be distinguished. In comparison the Tl^+, I^- peaks in the absence of a background gas were $50\text{-}100\times10^{-14}$ amps at a pressure of ~40μ thallium iodide, and considerably higher in the higher temperature experiments. The addition of nitrogen dioxide or sulfur hexafluoride greatly reduced the signal and in some cases the complex peaks were quite small, but generally easily distinguished from the noise and drift.

At a thallium iodide pressure of 40μ and with no inert gas present

Table V. Ions observed in the mass spectrometer
Temperature ≃ 630°K Pressure (TlI) ≃ 40μ

TlI	TlI, SF_6	TlI, NO_2	Remove NO_2	Add SF_6	$TlNO_3$	TlI, $TlNO_3$
1.85 (1.82)	1.85 (1.82)	1.85 (1.82)	1.85 (1.82)	1.85 (1.82)	no	1.87 (1.82)
Tl^+	Tl^+ [100]	Tl^+ [2]	Tl^+	Tl^+ [1]	peaks	Tl^+ [10]
					observed	
	1.14 (1.125)	1.16-1.25 (1.20)		1.2 (1.20)		1.23 (1.20)
	Tl_2^+I [10]	$Tl_2^+NO_3$ [1]		$Tl_2^+(NO_3)$ [1]		$Tl_2^+(NO_3)$ [1]
2.37 (2.32)	2.35 (2.32)	2.35 (2.32)	2.35 (2.32)	2.35 (2.32)		2.35 (2.32)
I^-	I^- [100]	I^- [1]	I^- [2]	I^- [2]	no	I^- [10]
		3.35 (3.31)	3.35 (3.31)	3.35 (3.31)	peaks	3.35 (3.31)
	1.22 (1)	NO_3^- [2]	NO_3^- [1]	NO_3^- [2]	observed	NO_3^- [20]
	TlI_2^- [1]					
		1.46 (1.43)		1.45 (1.43)		1.46 (1.43)
		$Tl(NO_3)_2^-$ [3]		$Tl(NO_3)_2^-$ [7]		$Tl(NO_3)_2^-$ [10]

Table VI Ions observed in the Mass Spectrometer
Temperature ≃ 720°K Pressure ≃ 1 torr

TlI	TlI, NO_2		Remove NO_2	
.89 (.886) (weak)	.89 (.886)		.89 (.886)	
Tl^+ $(TlI)_2$	$Tl^+(TlI)_2$	[1]	$Tl^+(TlI)_2$	[10]
1.13 (1.125)	1.13 (1.125)		1.13 (1.125)	
Tl_2^+I	Tl_2^+I	[120]	Tl_2^+I	[600]
	1.83 (1.82)		1.25 (1.22)	
	Tl^+	[50]	TlI_2^+	[8]
	2.32 (2.32)		2.32 (2.32)	
	I^+	[5]	I^+	[2]
1.83 (1.82)				
Tl^+	4.2 (see text)	[3]	1.83 (1.82)	
			Tl^+	[230]
.93 (.925) (weak)	.98 (.977)		.93 (.925)	
$(TlI)_2I^-$	$(TlI)_2NO_3^-$	[10]	$(TlI)_2I^-$	[20]
1.22 (1.22)	1.22 (1.22)		1.22 (1.22)	
TlI_2^-	TlI_2^-	[150]	TlI_2^-	[400]
	1.31 (1.31)			
	$TlI\ NO_3^-$			
2.32 (2.32)	2.32 (2.32)		2.32 (2.32)	
I^-	I^-	[40]	I^-	[100]
	3.32 (3.31)		3.32 (3.31)	
	NO_3^-	[5]	NO_3^-	[10]

the only peaks observed were Tl^+ and I^-. With the addition of sulfur hexafluoride at a pressure of approximately one torr peaks corresponding to the complexes Tl_2^+I and TlI_2^- also appeared. The complexes are probably formed by a three body mechanism whose rate we can write as

$$\frac{d(Tl_2^+I)}{dt} = k_3(M)\ (TlI)\ (Tl^+) \qquad (IV.4)$$

where (M) is the sulfur hexafluoride concentration and k_3 is the three body rate constant. For the pressures in the spectrometer (M)(TlI) = $10^{31}/cm^6$ and Eq. (IV.4) gives

$$(Tl_2^+I) = k_3 10^{31}(Tl^+)t \qquad (IV.5)$$

At one torr pressure the ions remain in the spectrometer for about one millisecond (see part B, section 3) and since the ions seen were up to 10% complexes we can estimate that $k_3 = 10^{-29}$.

The experiments done at a thallium iodide pressure of one torr with no inert gas present gave rise to the further complexes $Tl_3^+I_2$ and $Tl_2I_3^-$. In this case the single complexes Tl_2^+I and TlI_2^- were the dominant ions present; the atomic ion peaks were about four times smaller and the peaks of the double complexes $Tl_3^+I_2$ and $Tl_2I_3^-$ were about 5% those of the single complexes.

There are several ways in which the double complexes can be formed:

$$Tl_2^+I + TlI + M \longrightarrow Tl_3^+I_2 + M \qquad (IV.6)$$

$$Tl^+ + (TlI)_2 + M \longrightarrow Tl_3^+I_2 + M \qquad (IV.7)$$

and similar reactions for the negative ions. Equation (IV.6) depicts a three body reaction starting from the single complex. In this case M represents the thallium iodide molecule at a pressure of one torr and

(TlI) is 25 times larger than in the experiments at a pressure of 40μ. If the rate constant for Eq. (IV.6) is approximately the same as that in Eq. (IV.4), reaction according to Eq. (IV.6) could easily be expected to produce the observed double complexes.

Equation (IV.7) indicates a three body mechanism starting from the atomic ions and thallium iodide dimers. Cubicciotti[5] has estimated that the dimer concentration is less than 1% of the monomer at thallium iodide pressures between one torr and one atmosphere. If the three body rate constants for reactions (IV.6) and (IV.7) are similar, double complexes formed from the dimers should be of little importance.

Double complexes can also be formed if the lifetime of the metastable ion formed from collision of either the atomic ion with the dimer, or a single complex with a thallium iodide molecule, is long compared with the collision frequency. This process is important at high pressures where the metastable ion can become collisionally deactivated before it breaks apart again. Since Eq. (IV.6) is adequate to explain the experimental results, the importance of this mechanism is indeterminate.

Upon addition of nitrogen idoxide to the spectrometer a peak corresponding to NO_3^- was observed. In no instance was there any indication of the presence of any NO_2^- although it was expected on the basis of the equilibrium and kinetic calculations of Chapter II and from the fact that the reaction

$$Cl^- + NO_2 \longrightarrow Cl + NO_2^- \qquad \text{(IV.8)}$$

has been observed by Curran[6] in a mass spectrometer ion source. The electron affinity of Cl is .55 ev larger than that of I so the equilibrium is more favorable to NO_2^- in the corresponding reaction with I^-.

There are several possible mechanisms for the formation of NO_3^-; (1) a direct charge exchange between I^- and NO_3,

$$I^- + NO_3 \xrightarrow{k_1} I + NO_3^- \qquad (IV.9)$$

and (2) the formation of NO_2^- and its subsequent conversion to NO_3^-,

$$NO_2 + I^- \xrightarrow{k_2} I + NO_2^- \qquad (IV.10)$$

$$NO_2^- + NO_2 \xrightarrow{k_3} NO_3^- + NO \qquad (IV.11)$$

The first mechanism requires the presence of a sufficient amount of NO_3. At the temperatures in the spectrometer (600°K-720°K) NO_2 is unstable with respect to NO and O_2. Two possible methods for its decomposition are[7]

$$NO_2 + NO_2 \longrightarrow NO + O_2 + NO \qquad (IV.12)$$

and

$$NO_2 + NO_2 \longrightarrow NO_3 + NO \qquad (IV.13)$$

$$NO_3 + NO_2 \longrightarrow NO_2 + O_2 + NO \qquad (IV.14)$$

From the thermodynamic quantities for NO_3,[8] one can calculate for reaction (IV.13), $\Delta H^o = 23$ kcal, $\Delta S^o = -5$ eu, $K_{eq} = 10^{-8}$ at 707°K. From the equilibrium constant we find that the highest possible $(NO_3)/(NO_2)$ ratio is 10^{-4} at 707°K and since the pressure of NO_2 was less than 100μ, the pressure of NO_3 was less than .01μ. In order for reaction (IV.9) to be the dominent mechanism its rate constant (k_1) would have to be 5-6 orders of magnitude larger than that of reaction (IV.10). The requirements of the second mechanism however are not as stringent. If $k_3 \gg k_2$, the ratio $(NO_2^-)/(I^-)$ is equal to the ratio k_2/k_3, and if $k_3 \gtrsim 100k_2$ it would be difficult to detect any NO_2^- in the spectrometer. This mechanism and the conditions on the ratio k_2/k_3 are quite reasonable if the electron

affinity of NO_3 is greater than that of NO_2 (i.e. > 4.0 ev[9]).

When NO_2 was removed from the spectrometer the NO_3^- peak persisted. In order to determine its origin experiments were done with thallium nitrate alone, which yielded no detectable ions when photolyzed with the same 2062 Å radiation, and with a mixture of thallium iodide and thallium nitrate which yielded the NO_3^- peak again as well as the atomic Tl^+ and I^- peaks and the complexes $Tl_2^+(NO_3)$ and $Tl(NO_3)_2^-$. NO_3^- is apparently formed through collision of I^- and $TlNO_3$, i.e.,

$$I^- + TlNO_3 \longrightarrow (TlI)^* + NO_3^- \qquad \text{(IV.15)}$$

where the products other than NO_3^- are unknown. This is important since it indicates that $TlNO_3$ formed in the recombination experiments provided an increasing source of NO_3^- ions whether or not NO_2 remained throughout the experiment.

In the high temperature experiments peaks were also observed for I^+ and TlI_2^+. The latter peak could be either I^+ complexed on TlI or Tl^+ complexed on I_2. The pink color of the silicone grease in stopcocks near the spectrometer indicated that a significant quantity of I_2 may have been formed and since the intensity of the I^+ was low the TlI_2 peak was more likely Tl^+ complexed on I_2. The ionization potential of I is 10.45 ev[10] and since the 2062 Å radiation corresponds to only 6 ev it is difficult to explain the origin of the I^+ ions. If enough stray light had gotten into the accelerator region photo-electrons produced from the accelerator electrode and accelerated through 400 volts may have been the origin of the needed energy to produce the I^+ ions.

A peak of weak intensity at 4.2 Mc corresponding to a mass of 38.5±1 was observed when NO_2 was added and disappeared when the NO_2 was removed. This frequency also corresponds to one of the small side peaks of I^+. Its origin remained unexplained.

B. Estimates of Complex Formation

It is possible to make some crude estimate of the stability, equilibrium concentration and rate of formation of some simple ion complexes. For this purpose we give in Table VII, atomic and molecular constants pertinent to the calculations. The polarizabilities given for the halides are really lower limits since the thallium halides are largely ionic[11] and the halide ion polarizabilities are larger than those of the corresponding atom. It is also unlikely that the thallium iodide dipole moment is zero, consequently the corresponding equilibrium constant should be a lower limit.

1. Ion-parent Molecule Complexes

We consider first the atomic ion complexed on the parent molecule. For thallium iodide with $\mu_D = 0$ the most stable complexes are

```
Tl-I          Tl-I
 \ /           \ /
  I-            Tl+
```

We assume for simplicity that all bond distances have the molecule equilibrium value. For the bromide and chloride, because of the large permanent dipole moment, the most stable complexes are

$$Tl^{+}\text{-}X\text{-}Tl \qquad\qquad X^{-}\text{-}Tl\text{-}X$$

An ion and molecule, at large separation R, have an interaction energy given by

$$U = -\frac{\alpha e^2}{2R^4} \qquad \text{(IV.16)}$$

when α is the polarizability of the molecule.

If we assume that the ion interacts separately with each atom in the molecule according to this law we can calculate the polarizability interaction. Also, taking into account the ion permanent dipole moment

Table VII. Atomic and molecular constants

	r_e (Å) [a]	ω_e (cm^{-1}) [a]	μ_o (Debyes)		polarizability × 10^{24} (cm^3)
TlI	2.87	150	~0 [b]	Tl	5.0 [d]
TlBr	2.68	192.1	4.3 [c]	I	4.0 [e]
TlCl	2.55	456.4	4.6 [b]	Br	2.48 [e]
				Cl	1.63 [e]

[a] Reference 12

[b] Reference 13

[c] Reference 11

[d] Estimated from the value for Hg (ref. 14) and Pb^{++} (ref. 15).

[e] Reference 15 (we assume the halide polarizabilities are equal to those of the corresponding noble gas.

interaction we can calculate the bond energy of the complex given in column two of Table VIII.

The equilibrium constant for the reaction

$$TlX + X^- = TlX_2^- \qquad (IV.17)$$

is

$$K = \frac{[TlX_2^-]}{[TlX][X^-]} = \frac{f_{TlX_2^-}/V}{f_{TlX}/V \quad f_{X^-}/V} e^{\Delta E/kT} \qquad (IV.18)$$

where f is the partition function measured from the lowest electronic state assuming that state to be the only important one. $(-\Delta E)$ is the bond energy of the complex.

We first consider the linear complexes. Using the local properties method,[16] we write Eq. (IV.18) as

$$K = r_e^2 \left(\frac{2\pi kT}{F_{r_e}}\right)^{1/2} \left(\frac{2\pi kT}{F_\theta}\right) e^{\Delta E/kT} \qquad (IV.19)$$

where F_{r_e} is the diatomic molecule force constant which we assume for both bonds and F_θ is the bending force constant. If we approximate F_θ by the values obtained for $HgBr_2$ (41 cm^{-1})[17] and $HgCl_2$ (70 cm^{-1}),[17] we find $F_\theta \sim kT$ and we can replace $(2\pi kT/F_\theta)$ by approximately 2π without making significant error. The formula for positive ion complexes is analogous.

For the iodide complex the situation is more complex. As an estimate we can again replace the volume factor for the ion in the complex by $2\pi r_e^2 \, (2\pi kT/F_{r_e})^{1/2}$. This is admittedly rather crude but from the last section we have direct evidence for the existence of the iodide complex in any case. The calculated equilibrium constants are given in column three of Table VIII. Using the vapor pressures from Fig. 3, we can obtain

Table VIII Ion-parent molecule equilibrium constants

Complex	bond energy (ev)	equilibrium constant (cm^3)	$\frac{[\text{ion complex}]}{[\text{ion}]}$
Tl_2I^+	.955	1.27×10^{-14}	1.10×10^{-1}
TlI_2^-	.955	1.27×10^{-14}	1.10×10^{-1}
Tl_2Br^+	1.295	1.84×10^{-12}	3.01×10^{2}
$TlBr_2^-$	1.623	1.19×10^{-9}	1.95×10^{5}
Tl_2Cl^+	1.391	2.03×10^{-12}	1.03×10^{3}
$TlCl_2^-$	1.930	5.70×10^{-8}	2.85×10^{7}

the ratio of complex ion to atomic ion concentrations. These are given in column four of Table VIII.

The calculations given here are crude and the equilibrium constants could easily be several orders of magnitude in error. In particular, because the thallium iodide dipole moment probably is not zero the corresponding complexes should be considerably more stable. Also, the bond distances in the complexes could be considerably larger than in the neutral thallium halide molecule and this could significantly reduce the calculated bond energy. Finally, the potentials for charge-dipole and charge-induced-dipole interactions are not valid for such small internuclear distances. In view of these severe limitations the calculated equilibrium constants have little quantitative accuracy although they indicate that the ions are more likely to exist as complexes than as free atomic ions.

2. Ion Neutral Complexes

Fueno, Eyring, and Ree (FER)[18] derived an expression for the equilibrium constant for the reaction

$$M + A^{\pm} = MA^{\pm} \qquad \text{(IV.20)}$$

where M is a neutral gas molecule. Under the rigid rotator and harmonic oscillator approximations and assuming that neither the rotational or vibrational energies can exceed the bonding energy ϵ_m, FER obtained the following expression for the equilibrium constant:

$$K = \frac{h^3}{(2\pi\mu kT)^{3/2}} \; \frac{8\pi^2 \mu r_m^2 kT}{h^2} \; \frac{[1-\exp(-\epsilon_m/kT)]^2}{[1-\exp(-\epsilon_v/kT)]} \; \exp(\epsilon_m/kT) \qquad \text{(IV.21)}$$

where μ is the reduced mass of the complex $MA^{\pm}$, r_m is the equilibrium internuclear distance between M and $A^{\pm}$, ϵ_m is the binding energy of the complex, and ϵ_v is the vibrational quantum of the $MA^{\pm}$ bond.

The interaction potential is approximated by the sum of the Lennard-Jones potential of interaction between the two neutral molecules and the polarization energy, i.e., the attraction between the static charge on $A^{\pm}$ and the dipole moment induced on M [Eq. (IV.16)]

$$V(r) = 4\,\epsilon_o \left\{ \left(\frac{\sigma}{r}\right)^{12} - \left(\frac{\sigma}{r}\right)^{6} \right\} - \frac{\alpha e^2}{2r^4} \qquad \text{(IV.22)}$$

where σ and ϵ_o are the Lennard-Jones parameters for the interaction between A and M and α is the polarizability of M, and r is the internuclear distance between M and $A^{\pm}$.

The parameters, r_m, and ϵ_m, of the complex can be obtained by minimizing V(r) with respect to r. EFR give a method of obtaining ϵ_v if the parameters ϵ_o, σ, and α are known. Table IX gives the potential

THIS IS A BLANK PAGE

parameters σ, ϵ_o/k, α and the parameters r_m, ϵ_m, and ϵ_v calculated by the FER method. The last column gives the equilibrium constant obtained from Eq. (IV.21).

At 100 torr and 575°K the molecule number density is $1.7\times10^{18}/cm^3$. The ratios of complex ion to free ion obtained from the equilibrium constants in Table IX range from .001 to .02. While equilibrium constants obtained by the FER method are only approximate it is unlikely that they are in error by several orders of magnitude and consequently it is unlikely that a significant fraction of the ions are bound to the inert gas atoms. Thus ion neutral complexes probably do not contribute appreciably to the recombination processes although it is quite possible that they are the intermediate species in the formation of the more stable complexes with the parent molecules (see next section).

3. Rate Constants

In order to estimate the rate constants for the formation of complexes of the ions with their parent molecules, we assume the following mechanism

$$\text{(i)} \qquad M + A^{\pm} \rightleftarrows MA^{\pm}$$

$$\text{(ii)} \qquad MA^{\pm} + TlX \xrightarrow{k_2} TlXA^{\pm} + M$$

If $MA^{\pm}$ is a loose complex and M is in large excess compared to $A^{\pm}$ and TlX, then $MA^{\pm}$ will be in equilibrium with $A^{\pm}$ and M undisturbed by step (ii). We can then write

$$\frac{dn_{TlXA^{\pm}}}{dt} = k_2\,[MA^{\pm}][TlX]$$

$$= k_2\,K\,[M][A^{\pm}][TlX] \qquad \text{(IV.23)}$$

K is the equilibrium constant for step (i) calculated in the previous section, and $k_2 = \sigma v$ where σ is the reaction cross section and v is the relative velocity of TlX and $MA^{\pm}$. To get an estimate of the rate we approximate σ by the cross section corresponding to orbiting of the ion complex and parent molecules (see reference 8 of Chapter V), i.e.,

$$\sigma = 2\pi \left(\frac{\alpha e^2}{\mu v^2}\right)^{1/2} \qquad \text{(IV.24)}$$

where α is the polarizability of TlX, μ is the reduced mass of the (TlX, $MA^{\pm}$) pair, and v is their relative velocity.

In the recombination experiments, thallium iodide had the smallest concentration, and consequently the smallest rate of complex formation. With $\mu \simeq 2\times10^{-22}$, $\alpha = 5\times10^{-24}$, $K \simeq 10^{-21}$, $[TlI] \simeq 10^{13}/cm^3$ and at 100 torr ($[M] = 1.7\times10^{18}/cm^3$), Eq. (IV.23) becomes

$$\frac{dn_{TlIA^{\pm}}}{dt} \cong 10\ [A^{\pm}] \qquad \text{(IV.25)}$$

While this implies that the characteristic time for the formation of the complex is approximately 100 msec, the results from the mass spectrometer imply a considerably smaller characteristic time. The inert gas pressure in the mass spectrometer was two order of magnitude smaller than in the recombination experiments while both the thallium iodide concentration and the concentration of ions were an order of magnitude higher. Thus the rates of formation of the complex should be similar. The mobility of the ions at 1 torr $\approx$ 1000 cm^2/volt·sec and at ~1 volt/cm between electrodes A and B (Fig. 15), the ions remain in the spectrometer for only ~1 msec. The fact that ion complexes were seen in appreciable concentrations (especially for Tl_2^+ I) indicates that the above estimate of the rate is too low and that the ions are appreciably complexed in a

few milliseconds.

The pressures in the experiments with thallium bromide and thallium chloride were an order of magnitude greater than with thallium iodide and is thus a more favorable condition for complex formation. It appears reasonable to assume therefore that the ions initially formed by photolysis are quickly complexed with the parent molecules probably in less than a few milliseconds. The possibility of further complexing $[A^{\pm}(TlX)_n]$ is difficult to estimate (see next section).

C. Diffusion Constants

A study of the diffusion parameters obtained from the numerical fits to the rate curves provides a further method of identifying the ions. The fact that a rate curve could be fit with a single diffusion constant indicates that there was not a significant change in the types of ions present during the time interval studied.

Diffusion studies have the disadvantage that there are no accurate theoretical predictions with which to compare experimental results, especially for high molecular weight complexes. The Langevin theory[20] provides the most generally satisfactory predictions of the mobility and diffusion constants. This entirely classical theory takes into account inverse-fifth-power ion-molecule attractive forces and rigid sphere repulsion but it neglects dispersion forces.

Langevin theory yields an equation for the mobility of the form

$$K = \frac{A}{[4\pi\alpha M_r]^{1/2}} \frac{1}{N} \qquad \text{(IV.26)}$$

where M_r is the reduced mass of the ion-molecule pair, α is the polarizability of the molecule, N is the molecule number density and A is a function of a parameter λ defined by the equation

$$\lambda^2 = kT\Big/\left(\frac{\alpha e^2}{2D_{12}^4}\right) \qquad \text{(IV.27)}$$

where D_{12} is the sum of the radii of the ion and molecule. λ^2 is equal to kT divided by the energy of attraction when the ion and molecule are in contact. Values of A for different values of λ are available in tabular form.[21] The ambipolar diffusion constant is obtained from Eqs. (III.8) and (III.18). When polarization forces completely predominate $\lambda = 0$, and $A = 0.5105$. As D_{12} increases, A first increases to a maximum for $\lambda \cong .6$ and then decreases for further increase in D_{12}.

Table X presents the ambipolar diffusion parameters determined from experiment as well as the values obtained from the Langevin theory both for the complete Langevin equation [Eq. (IV.26)] and in the polarizability limit. For the atomic ions, D_{12} is assumed to be the sum of the ionic radius of the ion and the atomic radius of the neutral. For the complexed ions we assume linear complexes having the structure

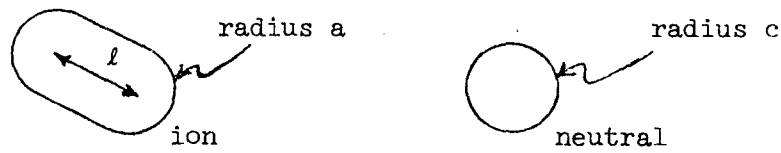

The "hard sphere" cross section for the ion-neutral is a function of the orientation of the ion. It is easily shown that the cross section averaged overall orientations is

$$\langle\sigma\rangle = \ell(a+c)\,\frac{\pi}{2} + \pi(a+c)^2 \qquad \text{(IV.28)}$$

This value was used in Eq. (IV.27) for πD_{12}^2. Columns six and seven give calculated values of the diffusion parameter for two sets of values of ℓ. In column six, ℓ is assumed to be twice the equilibrium internuclear

Table X. Ambipolar diffusion parameter $C \times 10^{-15}$ (1/cm sec deg)

System	Third Body	Langevin polarization limit		Complete Langevin equation			Experimental
		Tl^+ X^-	Tl_2^+X TlX_2^-	Tl^+ X^-	Tl_2^+I [a] TlI_2^-	Tl_2I [b] TlI_2^-	
TlI	Xe	1.89	1.58	2.18	1.70	1.62	1.47±.1
TlBr	Xe	2.01	1.60	2.31	1.74	1.67	1.54±.1
TlCl	Xe	2.26	1.65	2.60	1.81	1.74	1.55±.1
$TlI-NO_2$	Xe	2.17	1.63				1.31±.1
TlI	Ar	4.46	4.14	5.06	3.85	3.58	3.63±.1
TlBr	Ar	4.60	4.17	5.27	4.00	3.69	3.75±.1
TlCl	Ar	4.98	4.21	5.72	4.12	3.81	4.12±.1
$TlI-NO_2$	Ar	4.84	4.20				2.63±.1

[a] Internuclear distances from neutral molecule

[b] Internuclear distances from ionic crystals

distance in the thallium halide molecules (Table VII) and in column seven, ℓ is twice the internuclear distance calculated from the lattice spacing in the ionic crystals. Table XI gives the physical data used in the calculations.

The diffusion parameters obtained from the atomic ions are considerably higher than the experimental results especially when the "hard sphere" contribution is taken into account. In general, the best agreement is obtained for the complexes when the "hard sphere" contribution is included. Although in some cases agreement with experiment in column four is better than in column six or seven, neglect of the "hard sphere" contribution for such large complexes is unrealistic.

The somewhat low experimental values of the diffusion parameter for the case of xenon as a third body raises the question of the possibility of complexes of the form $A^{\pm}(TlX)_2$. The equilibrium constants for such complexes are not dependent on the inert gas, and the rate estimates indicate less than an order of magnitude increase in the rate of formation of the complexes in the case of xenon as a third body compared to argon. It therefore seems unlikely that complexes would be present for one inert gas and not the other. The strongest evidence against the existence of complexes of the form $A^{\pm}(TlX)_n$ where $n > 1$, is that fact that they would probably reduce the diffusion parameter well below the experimental value. A further doubling of the "hard sphere" cross section decreases the diffusion constant by 30-40%. While a single additional TlX molecule would not double the cross section, the increase coupled with the reduction due to the increased mass would reduce the calculated value considerably below the experimental result.

Table XI. Atomic and ionic radii
Thallium halide bond distance in the ionic crystal

Atomic and ionic radii (Å)	TlX bond distance in the ionic crystals (Å) [d]
Xe (1.9)[a]	TlCl (3.32)
Ar (1.54)[a]	TlBr (3.44)
Tl^+ (1.48)[b]	TlI (3.62)
I^- (2.19)[c]	
Br^- (1.95)[c]	
Cl^- (1.81)[c]	

[a] Reference 23

[b] The halide ionic radius was subtracted from the ionic crystal TlX bond distances to obtain a Tl^+ ionic radius. The value given is an average for the three thallium halides.

[c] Reference 24

[d] Reference 22

In view of the approximate nature of the "hard sphere" concept, the difficulty in estimating effective ionic radii and the high sensitivity of the Langevin theory to the resulting cross sections, as well as the fact that dispersion forces have been entirely neglected, agreement with experiment can be considered satisfactory and the assumption that the atomic ions are bound to a single thallium halide molecule is consistent with the diffusion results.

The thallium iodide experiments done with the addition of nitrogen dioxide are more difficult to interpret. Table V indicates that in all cases where complexes were seen with either nitrogen dioxide or thallium nitrate present, peaks were observed for the complexes $Tl_2^+NO_3$ and $Tl(NO_3)_2^-$ but not complexes of thallium iodide. The fact that the presence of thallium nitrate alone is sufficient to convert the Tl^+, I^- ions into $Tl_2^+(NO_3)$ and $Tl(NO_3)_2^-$ is strong evidence indicating that in the recombination experiments with NO_2 it was these ion complexes that were undergoing recombination. The first experiments with nitrogen dioxide used xenon as the neutral gas and consistent results were obtained only after many experiments were performed. It is reasonable that only in the later experiments was there sufficient $TlNO_3$ to produce the nitrate complexes and that in the earlier experiments mixtures of thallium iodide and thallium nitrate complexes were obtained.

Due to the difficulty in estimating the "hard sphere" cross sections for the nitrate complexes, the low value of the experimental diffusion parameter for the nitrogen dioxide experiments could be attributed to the expected large cross sections or possibly to complexes of the form $A^{\pm}(TlNO_3)_n$. The latter case is more likely in the experiments with argon, which were done last when more thallium nitrate had

been formed, and which showed the smallest diffusion constant for all the argon experiments. In conclusion, experimental results indicate that the most probable ions present in the nitrogen dioxide experiments were the complexes $Tl_2^+(NO_3)$ and $Tl(NO_3)_2^-$, although the possibility of further complexing of the form $A^{\pm}(TlNO_3)_n$, $n > 1$, cannot be eliminated especially for the argon experiments.

References for Chapter IV

1. A. N. Terenin and B. Popov, Phys. Z. Sow. 2, 299 (1932).

2. P. J. Feibelman, J. Chem. Phys. 43, 2462 (1965).

3. R. L. F. Boyd and D. Morris, Proc. Phys. Soc. A68, 1 (1955).

4. P. Harteck, R. R. Reeves, Jr., and B. A. Thompson, Z. Naturforsch. 19a, 2 (1964).

5. D. Cubicciotti, J. Phys. Chem. 69, 1410 (1965).

6. R. K. Curran, Phys. Rev. 125, 910 (1962).

7. N. Davidson and G. L. Schott, J. Chem. Phys. 27, 317 (1957).

8. G. Schott and N. Davidson, J. Amer. Chem. Soc. 80, 1841 (1958).

9. A. L. Farragher, F. M. Page, and R. C. Wheeler, Discussions Faraday Soc. 37, 203 (1964).

10. V. I. Vedeneyev et al., Bond Energies, Ionization Potentials and Electron Affinities (St. Martin's Press, New York, 1966), p. 152.

11. K. S. Krasnov, Russion J. of Inorg. Chem. 5, 805 (1960).

12. G. Herzberg, Spectra of Diatomic Molecules (Van Nostrand, New York, 1950) 2nd Ed.

13. A. L. McClellan, Tables of Experimental Dipole Moments (W. H. Freeman, San Francisco, 1963).

14. Landolt-Börnstein, Physikalisch-Chemische Tabellen (Springer-Verlag, Berlin, 1950), 6th Ed.

15. A. Dalgarno, Advan. Phys. 11, 281 (1962).

16. D. R. Herschbach, H. S. Johnston, and D. Rapp, J. Chem. Phys. 31, 1652 (1959).

17. W. Klemperer, J. Electrochem. Soc. 110a, 1023 (1963).

18. T. Fueno, H. Eyring, and T. Ree, Can. J. Chem. 38, 1693 (1960).

19. J. O. Hirschfelder, D. F. Curtiss, and R. B. Bird, Molecular Theory of Gases and Liquids (John Wiley and Sons, Inc., New York, 1954), pp. 1110-1111.

20. P. Langevin, Ann. Chim. Phys. 28, 289 (1903).

21. E. W. McDaniel, Collision Phenomena in Ionized Gases (John Wiley and Sons, Inc., New York, 1964), p. 433.

22. H. Remy, Treatise on Inorganic Chemistry (Elsevier Publishing Co., New York, 1956), Vol. 1, p. 383.

23. T. Moeller, Inorganic Chemistry (John Wiley and Sons, Inc., London, 1952).

24. J. C. Slater, J. Chem. Phys., 41, 3199 (1964).

V. THEORY OF IONIC RECOMBINATION AND COMPARISON WITH EXPERIMENT

A. Mechanisms of Ionic Recombination

In "recombination" experiments, what is actually measured in the disappearance of ions and not necessarily their recombination. This may take place according to one or more of the following reactions:

$$X^+ + Y^- \rightarrow XY + h\nu \tag{V.1}$$

$$X^+ + Y^- \rightarrow X^* + Y^* \tag{V.2}$$

$$X^+ + Y^- + M \rightarrow XY + M \tag{V.3}$$

Radiative recombination [Eq. (V.1)] is a very ineffective process. The time an ion requires to transverse a typical molecular diameter is about 10^{-12} seconds and since measured lifetimes of excited states are about 10^{-8} seconds we can estimate the probability that a photon will be emitted in a single collision at about 10^{-4}/sec. This corresponds to a recombination coefficient of about 10^{-14} cm^3/sec. or five to six orders of magnitude smaller than experimental results.

Bimolecular recombination [Eq. (V.2)] results when two ions get sufficiently close to allow the electron to be transferred from the negative to positive ion. In the case of atomic ions internal energy is converted into relative kinetic energy and the atoms depart either in their ground or excited states. In complexed ions, however, the additional degrees of freedom may lead to a variety of processes depending on where the collision occurs on the potential energy surface (see Section C).

The recombination coefficient α can be written in the form

$$\alpha = \alpha_o + \alpha_p \tag{V.4}$$

where α_o is independent of pressure and includes the effect of radiative and bimolecular recombination. $\dot{\alpha}_p$, at low pressures (less than a few hundred torr), is linear in the third body pressure and described the effect of three body recombination [Eq. (V.3)]. Equation (V.4) is observed to hold experimentally in Figs. 10-13.

B. Three Body Recombination

1. Mechanism

The mechanism which has achieved the most success in describing three body recombination is that of collisional deactivation originally proposed by Thomson[1] in 1924. An ion pair whose motion is unbound may become bound through deactivating collisions of an ion and neutral third body. If the resulting orbit allows the ions to come sufficiently close for electron transfer to occur or if further third body collisions produce such an orbit an eventual "recombination" will take place. If an ion in a weakly bound orbit ($-E \lesssim kT$) undergoes an ion-neutral collision the ion pair will in general be dissociated while a strongly bound ion-pair ($-E \gtrsim kT$) will in general lose further internal energy on such collisions. At low pressures, the fate of a bound ion pair is determined in a few ion-neutral collisions[2] and is independent of the third body pressure. If the rate of formation of bound ion pairs and their dissociation and deactivation are taken into proper account the rate in principle can be calculated.

At very high pressures experiment[3] indicates that the recombination rate decreases with increasing pressure. Langevin[4] developed a simple theory based on the idea that the oppositely charged ions drift towards each other through the neutral gas at a rate determined by their mobilities, K^+ and K^-. The recombination coefficient determined by Langevin is given by

$$\alpha = 4\pi e^2(K^+ + K^-) \qquad (V.5)$$

and is in general agreement with experiment at high pressures (~10 atm.).

2. Determination of the Capture Radius

In order to simplify calculations on the mechanism discussed in the previous section, Thomson[1] assumed that all ions, at infinite separation, have their average thermal velocities and introduced the concept of a capture radius. According to Thomson recombination of positive and negative ions occur if and only if an ion undergoes a collision with a neutral thrid body when the ions are within a certain capture radius R_c. The capture radius is generally defined by the condition that the average relative energy of an ion pair after a collision with a third body at separation R_c is zero, i.e.,

$$\langle T_{rel} \rangle - \frac{e^2}{R_c} = 0. \qquad (V.6)$$

The recombination rate is then the number of ions per unit time which undergo collisions with neutrals when the ion-ion separation is less than the capture radius.

This model assumes that any ions that enter a bound state when $r < R_c$ are stably trapped and further collisions do not dissociate the ion pair. Thomson made some rather unjustified assumptions for the collisional dynamics, neglected the curvature of the ion paths, and obtained a rate which is in fairly good agreement with experiment. Natanson[5] made somewhat different assumptions for the collisional dynamics, obtained a smaller capture radius and also took into account the curvature of the ion paths. The effects approximately cancel and Natanson's results are again in good agreement with experiment. Natanson's

equations also take into account the effect of higher pressures and predict Eq. (V.5) exactly in the high pressure limit. Brueckner[6] corrected an error in Natanson's calculation and reduced the capture radius by a factor of 3/5. He also applied a more rigid stability criterion (other than Eq. (V.6)) and obtained a capture radius 4/15 that of Natanson.

In previous work the two masses were assumed to be equal. We derive here the capture radius for the case of different masses for the positive ion, negative ion, and third body, m_1, m_2, and m_3 respectively, and eliminate the one remaining assumption of Brueckner (see below Eq. (V.21). We use the zero energy stability criterion, i.e., Eq. (V.6).

Consider two ions, 1 and 2, of masses m_1 and m_2 moving initially at large separation with momenta $\underset{\sim}{P}_1^{(o)}$ and $\underset{\sim}{P}_2^{(o)}$ in the laboratory coordinate system (we use the notation of Brueckner). The momenta of the ions in the center of mass system are

$$\underset{\sim}{Q}_1 = \underset{\sim}{P}_1 - \frac{m_1}{m_1 + m_2}(\underset{\sim}{P}_1 + \underset{\sim}{P}_2) \tag{V.7}$$

$$\underset{\sim}{Q}_2 = -\underset{\sim}{Q}_1 \tag{V.8}$$

Now suppose ion 1 collides, while at separation r, with a neutral molecule of mass m_3 and the scattering of 1 on 3 is isotropic in the center of mass system of 1 and 3. The momentum of ion 1 in the 1-3 center of mass system before the collision is

$$\underset{\sim}{L} = \underset{\sim}{P}_1 - \frac{m_1}{m_1 + m_3}(\underset{\sim}{P}_1 + \underset{\sim}{P}_3) \tag{V.9}$$

$$= (m_3\underset{\sim}{P}_1 - m_1\underset{\sim}{P}_3)/(m_1 + m_3)$$

and after the collision

$$L' = |(m_3 \underset{\sim}{P}_1 - m_1 \underset{\sim}{P}_3)| \frac{\hat{n}}{m_1 + m_3} \tag{V.10}$$

where $\hat{n}$ is a randomly orientated unit vector. Equation (V.10) assumes additionally that "during" the ion-neutral collision the effect of ion 2 on ion 1 can be neglected (it is exact for hard spheres). The momentum of ion 1 after the collision is, in the laboratory system,

$$\underset{\sim}{P}_1' = \underset{\sim}{L}' + \frac{m_1}{m_1 + m_2} (\underset{\sim}{P}_1 + \underset{\sim}{P}_3) \tag{V.11}$$

and in the center of mass system of 1 and 2,

$$\underset{\sim}{Q}_1' = (m_2 \underset{\sim}{P}_1' - m_1 \underset{\sim}{P}_2)/(m_1 + m_2) \tag{V.12}$$

The relative kinetic energy is the sum of the relative kinetic energies of ions 1 and 2, i.e.,

$$T_{rel} = \frac{Q_1^2}{2m_1} + \frac{Q_2^2}{2m_2} = \frac{Q_1^2}{2\mu} \tag{V.13}$$

where μ is the reduced mass, $m_1 m_2/(m_1 + m_2)$. From Eqs. (V.12) and (V.13), we have

$$T_{rel}' = \frac{1}{2}\mu \left(\frac{\underset{\sim}{P}_1'}{m_1} - \frac{\underset{\sim}{P}_2}{m_2}\right)^2 \tag{V.14}$$

where the prime refers to the kinetic energy after the collision with the third body. If we substitute in Eq. (V.14) from Eqs. (V.10) and (V.11), and average over the directions of $\hat{n}$ and $\underset{\sim}{P}_3$ we obtain

$$T_{rel}' = \frac{1}{2}\mu \left\{ \frac{m_3^2}{m_1^2 (m_1 + m_3)^2} P_1^2 + \frac{2}{(m_1 + m_3)^2} P_3^2 + \left[\frac{\underset{\sim}{P}_1}{(m_1 + m_3)} - \frac{\underset{\sim}{P}_2}{m_2}\right]^2 \right\} \tag{V.15}$$

From conservation of energy

$$\frac{Q_1^{2(o)}}{2\mu} = \frac{Q_1^2}{2\mu} - \frac{\alpha}{r} \tag{V.16}$$

where α is the square of the electronic charge. From Eq. (V.7) in the form

$$\underset{\sim}{Q}_1^{(o)} = (m_2 \underset{\sim}{P}_1^{(o)} - m_1 \underset{\sim}{P}_2^{(o)})/(m_1 + m_2) \tag{V.17}$$

with the definitions

$$\underset{\sim}{P}_1 = \underset{\sim}{P}_1^{(o)} + \Delta \underset{\sim}{Q}_1$$

$$\underset{\sim}{P}_2 = \underset{\sim}{P}_2^{(o)} - \Delta \underset{\sim}{Q}_1 \tag{V.18}$$

we can obtain

$$\frac{\underset{\sim}{P}_2^{(o)} \cdot \Delta \underset{\sim}{Q}_1}{m_2} = \frac{\underset{\sim}{P}_1^{(o)} \cdot \Delta \underset{\sim}{Q}_1}{m_1} + \frac{\Delta Q_1^2}{2\mu} - \frac{\alpha}{r} \tag{V.19}$$

We now assume that in the laboratory coordinate system the ions, at infinite separation, and the third bodies have their average thermal energies, i.e.,

$$\frac{P_1^{2(o)}}{2m_1} = \frac{P^{2(o)}}{2m_2} = \frac{P_3^{\,2}}{2m_3} = \frac{3}{2}\,kT = T_o \tag{V.20}$$

Using Eqs. (V.18), (V.19), and (V.20), Eq. (V.15) becomes (after considerable manipulation)

$$T'_{rel} = T_o - \underset{\sim}{P}_1^{(o)} \cdot \underset{\sim}{P}_2^{(o)} \frac{\mu}{m_2(m_1 + m_3)}$$

$$+ \frac{\alpha}{r} \frac{m_1(m_1 + m_2 + m_3)}{(m_1 + m_2)(m_1 + m_3)} + \tag{V.21}$$

$$+\left(\frac{\underset{\sim}{P}_1^{(o)}\cdot\Delta\underset{\sim}{Q}_1}{\mu}+\frac{1}{2}\frac{\Delta Q_1^2}{\mu}\right)\left(1-\frac{2m_1m_2m_3(m_1+m_2+m_3)}{(m_1+m_2)^2(m_1+m_3)^2}-\frac{m_1(m_1+m_2+m_3)}{(m_1+m_2)(m_1+m_3)}\right)$$

Brueckner assumed $\langle\underset{\sim}{P}_1^{(o)}\cdot\Delta\underset{\sim}{Q}_1\rangle = \langle\underset{\sim}{P}_2^{(o)}\cdot\Delta\underset{\sim}{Q}_1\rangle = 0$ where the average is over the directions of $\underset{\sim}{P}_1^{(o)}$ and $\underset{\sim}{P}_2^{(o)}$. With this assumption Eq. (V.19) becomes

$$\left\langle\frac{\Delta Q_1^2}{2\mu}\right\rangle = \frac{\alpha}{r} \tag{V.22}$$

and for $m_1 = m_2$, Eq. (V.21) becomes

$$T'_{rel} = T_o - \underset{\sim}{P}_1^{(o)}\cdot\underset{\sim}{P}_2^{(o)}\frac{m_1}{2(m_1+m_3)} + \frac{\alpha}{2r}\left(1+\frac{m_1^2}{(m_1+m_3)^2}\right) \tag{V.23}$$

which is Brueckner's result.[6]

In order to eliminate the above assumptions, we need an expression for $\Delta\underset{\sim}{Q}_1$. We first write the relative velocity vector of the two ions, $\underset{\sim}{V}$, in terms of two vectors in the plane of motion, the initial relative velocity vector $\underset{\sim}{V}_{init}$ and the vector $\underset{\sim}{V}_{init}\times\underset{\sim}{M}$, where $\underset{\sim}{M}$ is the angular momentum. The equations of motion of two oppositely charged ions in a coulomb field are,[7] in aparmetric form

$$\begin{aligned} r &= a(e\cdot\cosh\xi - 1)\\ x &= a(e - \cosh\xi)\\ y &= a(e^2-1)^{1/2}\sinh\xi\\ t &= (\mu a^3/\alpha)^{1/2}(e\cdot\sinh\xi - \xi)\end{aligned} \tag{V.24}$$

where e, the eccentricity, is given by

$$e = \left(1+\frac{2EM^2}{\mu\alpha^2}\right)^{1/2} \tag{V.25}$$

and $a = \alpha/2E$. E is the relative energy and M is the angular momentum. From Eq. (V.24), we can obtain the formula

$$\underset{\sim}{V} = \underset{\sim}{V}_{init} \left\{ \mp \frac{1}{re^2} [(r+a)^2 - a^2e^2]^{\frac{1}{2}} + \frac{e^2-1}{e^2} \frac{r+a}{r} \right\}$$

$$+ \underset{\sim}{V}_{init} \frac{\underset{\sim}{M}}{M} \left\{ \mp \frac{\sqrt{e^2-1}}{re^2} [(r+a)^2 - a^2e^2]^{\frac{1}{2}} - \frac{\sqrt{e^2-1}}{e^2} \frac{r+a}{r} \right\} \tag{V.26}$$

where the lower sign refers to the incoming particles and the upper sign to the outgoing particles. Let

$$\underset{\sim}{V} = A \underset{\sim}{V}_{init} + B \underset{\sim}{V}_{init} \times \frac{\underset{\sim}{M}}{M} \tag{V.27}$$

since

$$\underset{\sim}{Q}_1 = \mu \underset{\sim}{V}$$

$$\Delta \underset{\sim}{Q}_1 = \mu(A-1) \underset{\sim}{V}_{init} + \mu B \underset{\sim}{V}_{init} \times \underset{\sim}{M}/M \tag{V.28}$$

From Eqs. (V.26), (V.27), and (V.28) we obtain

$$\frac{\Delta Q_1^2}{2\mu} = \frac{1}{2} \mu V_{init}^2 [(A-1)^2 + B^2]$$

$$= E[(A-1)^2 + B^2] \tag{V.29}$$

$$= \frac{\alpha}{r} - 2E(A-1)$$

and

$$\frac{\underset{\sim}{P}_1^{(o)} \cdot \Delta \underset{\sim}{Q}_1}{\mu} = (A-1) \frac{P_1^{2(o)}}{m_1} - (A-1) \frac{\underset{\sim}{P}_1^{(o)} \cdot \underset{\sim}{P}_2^{(o)}}{m_2} - B \left(\frac{\underset{\sim}{P}_1^{(o)} \times \underset{\sim}{P}_2^{(o)}}{m_2} \cdot \frac{\underset{\sim}{M}}{M} \right) \tag{V.30}$$

Equation (V.30) and hence Eq. (V.21) depend on the azimuthal angle, i.e., the orientation of the plane of motion of the ions. It arises due to the motion of the center of mass of the ions, for when the center of mass is

stationary, $\underset{\sim}{P}_1^{(o)} \times \underset{\sim}{P}_2^{(o)} = 0$ and Eq. (V.30) only depends on the magnitude of $\underset{\sim}{M}$(through A). To proceed further we average over the azimuthal angle and since $\langle \underset{\sim}{M} \rangle = 0$ the last term in Eq. (V.30) drops out. From Eqs. (V.29), (V.30), and (V.20), (leaving out the last term in Eq. (V.30)) we can write Eq. (V.21) in the form

$$T'_{rel} = T_o - \underset{\sim}{P}_1^{(o)} \cdot \underset{\sim}{P}_2^{(o)} \frac{\mu}{m_2(m_1+m_3)}$$

$$+ \frac{\alpha}{r}\left[1 - \frac{2m_1m_2m_3(m_1+m_2+m_3)}{(m_1+m_2)^2(m_1+m_3)^2}\right] \tag{V.31}$$

$$+ (A-1)\underset{\sim}{P}_1^{(o)} \cdot \underset{\sim}{P}_2^{(o)} \frac{m_2-m_1}{m_2(m_1+m_2)}\left[1 - \frac{2m_1m_2m_3(m_1+m_2+m_3)}{(m_1+m_2)^2(m_1+m_3)^2} - \frac{m_1(m_1+m_2+m_3)}{(m_1+m_2)(m_1+m_3)}\right]$$

We now average over the directions of $\underset{\sim}{P}_1^{(o)}$ and $\underset{\sim}{P}_2^{(o)}$ and using Eq. (V.6), obtain

$$T_o - \frac{\alpha}{R_c} \frac{2m_1m_2m_3(m_1+m_2+m_3)}{(m_1+m_2)^2(m_1+m_3)^2} \tag{V.32}$$

$$+ \langle A\, \underset{\sim}{P}_1^{(o)} \cdot \underset{\sim}{P}_2^{(o)} \rangle \frac{m_2 - m_1}{m_2(m_1+m_2)}\left[1 - \frac{2m_1m_2m_3(m_1+m_2+m_3)}{(m_1+m_2)^2(m_1+m_3)^2} - \frac{m_1(m_1+m_2+m_3)}{(m_1+m_2)(m_1+m_3)}\right]$$

$$= 0$$

For collisions of m_2 and m_3, interchange m_1 and m_2.

When the positive and negative ions have equal masses, $m_1 = m_2$, and the last term in Eq. (V.32) is zero. In this case Eq. (V.32) gives the same result as that obtained by Brueckner although the assumptions made by Brueckner are invalid (compare Eqs. (V.22) and (V.29)).

Equation (V.32) is a function of the impact parameter, b, through

the last term. The average $\langle A \underset{\sim}{P}_1^{(o)} \cdot \underset{\sim}{P}_2^{(o)} \rangle$ was obtained numerically and Eq. (V.32) was solved for the capture radius as a function of the impact parameter. In Fig. 17 the capture radius is plotted as a function of b for the ions Tl^+, Cl^- and xenon as a third body. The upper set of curves represent collisions of Cl^- with Xe, while the bottom set are for collisions of Tl^+ with Xe. The upper curve in each set corresponds to the capture radius for the incoming particle, the lower curve for the outgoing particle and for the middle straight line we neglect the last term in Eq. (V.32).

It can be seen from Fig. 17 that the effect of the last term in Eq. (V.32) is quite small. Furthermore, its effect on the incoming particle is opposite to that for the outgoing particle and consequently the rate will be changed little. Neglecting the last term in Eq. (V.32), the capture radius for collisions of m_1 with m_3 is

$$R_c = \frac{\alpha}{T_o} \frac{2m_1 m_2 m_3 (m_1+m_2+m_3)}{(m_1+m_2)^2 (m_1+m_3)^2} \tag{V.33}$$

Again, for collisions of m_2 with m_3, interchange m_1 and m_2.

The energy transfered in the collision of two particles is generally a maximum when the particles have equal mass. The effect of such mass matching is illustrated in Fig. 18 where the capture radius (Eq. (V.33)) is plotted vs the third body mass for different ion pairs. When one ion is considerably lighter than the other, the lighter ion, in the center of mass coordinate system, has most of the relative kinetic energy and is most effective in removing internal energy in ion-neutral collisions. This is illustrated in Fig. 18 for the case of Tl^+, Cl^-.

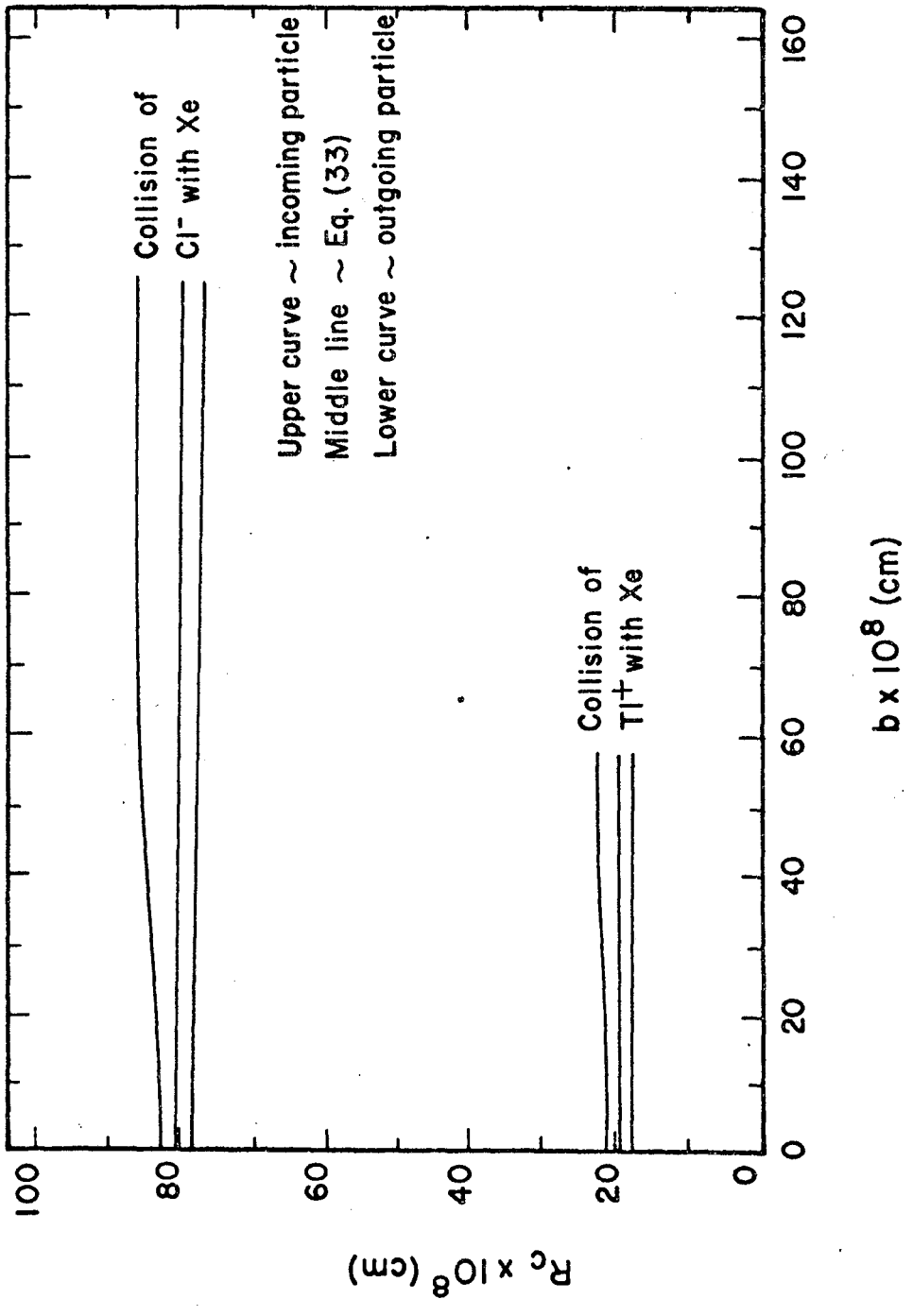

Fig. 17 Capture radius (R_c) vs impact parameter (b) for the system Tl, Cl^-, Xe

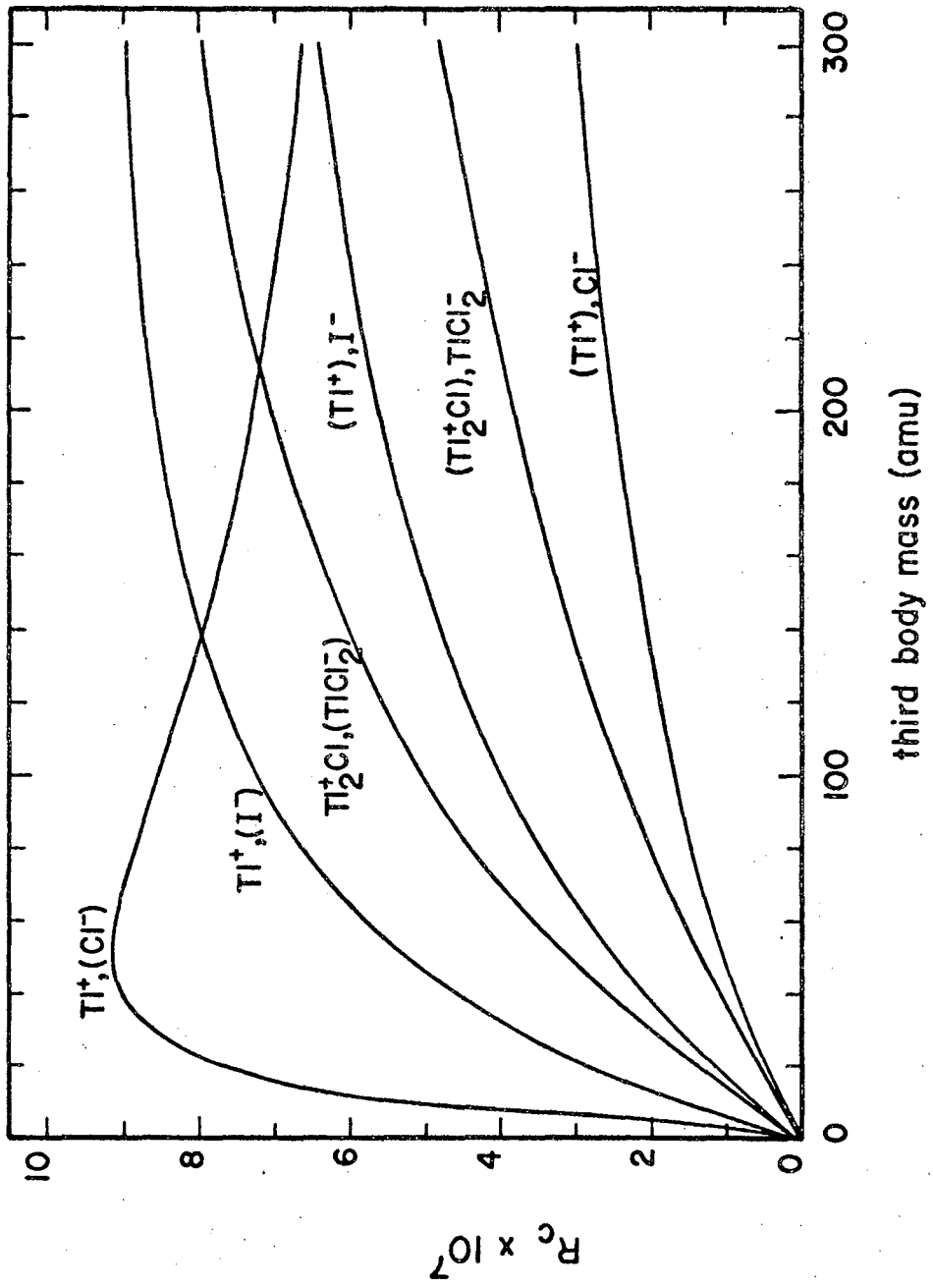

Fig. 18 The capture radius for different ion pairs vs the third body mass. The third body collides with the ion given in parenthesis. The temperature is 610°K.

3. Rate Constant

The three body recombination rate can be written in the form

$$\frac{dn^{\pm}}{dt} = - n_+ n_- \, 2\pi \int bdb \, | \underset{\sim}{V}_1^{(o)} - \underset{\sim}{V}_2^{(o)} | \, x$$

$$\left\{ \int_{-\infty}^{\infty} dt \, \frac{|\underset{\sim}{V}_1(t) - \underset{\sim}{V}_3|}{\lambda_1} \eta_1 + \int_{-\infty}^{\infty} dt \, \frac{|\underset{\sim}{V}_2(t) - \underset{\sim}{V}_3|}{\lambda_2} \eta_2 \right\} \quad (V.34)$$

where the ions at infinite separation and the neutral third bodies are assumed to have their average thermal energies. The factor $n_- 2\pi bdb \, |\underset{\sim}{V}_2^{(o)} - \underset{\sim}{V}_1^{(o)}|$ is the flux of negative ions on a single positive ion with a given impact parameter b. The two factors in brackets represent the probability that either a negative or positive ion will undergo a collision with the neutral third body in such a way as to bind the ions stably.

The mean free path λ_1 is defined such that $|\underset{\sim}{V}_1 - \underset{\sim}{V}_3|/\lambda_1$ is the probability per unit time that an ion of velocity $\underset{\sim}{V}_1$ collides with a neutral of velocity $\underset{\sim}{V}_3$. If $\eta(\underset{\sim}{V}_1, \underset{\sim}{V}_2, \underset{\sim}{V}_3, b, t)$ is the probability that for given values of the arguments the collision of 1 and 3 lead to a bound ion pair, then

$$\int dt \, \frac{|\underset{\sim}{V}_1 - \underset{\sim}{V}_3|}{\lambda_1} \eta_1 \quad (V.35)$$

represents the probability that the ion-ion collision at impact parameter b leads to a "recombination" through collisions of ion 1 with the neutral. The other term in Eq. (V.34) considers collisions of ion 2 with the neutral. The recombination coefficient obtained from Eq. (V.34) is

$$\alpha = 2\pi \int bdb |\underset{\sim}{V}_1^{(o)} - \underset{\sim}{V}_2^{(o)}| \left\{ \int_{-\infty}^{\infty} dt \, \frac{|\underset{\sim}{V}_1 - \underset{\sim}{V}_3|}{\lambda_1} \eta_1 + \int_{-\infty}^{\infty} dt \, \frac{|\underset{\sim}{V}_2 - \underset{\sim}{V}_3|}{\lambda_2} \eta_2 \right\}$$

(V.36)

Using the concept of a capture radius we can write

$$\eta_1 = \begin{cases} 1 & r \leqq R_1 \\ 0 & r > R_1 \end{cases}$$

$$\eta_2 = \begin{cases} 1 & r \leqq R_2 \\ 0 & r > R_2 \end{cases} \qquad (V.37)$$

where R_1 and R_2 are the respective capture radii for collisions of ions 1 and 2 with the neutral.

The mean free path λ, equals $1/N\sigma$ where N is the neutral number density and σ is the ion-neutral cross section. It has been customary to assume for simplicity that the ions travel straight line paths through the capture region, i.e., for $r < R_c$. It is not necessary to make this assumption when treating xenon as a third body. In this case Eq. (V.34) can be evaluated analytically.

The orbiting cross section for ion-neutral collisions, which is inversely proportional to the ion-neutral relative velocity is probably nearly isotropic and in the case of xenon, the polarizability is large enough that the orbiting cross section is larger than the average hard sphere cross section except for small ion-ion separations where the ions are moving very fast. The worst case is for collisions of TlI_2^- with Xe where the ion-ion separation at which the average hard sphere cross section is equal to the orbiting cross section is 22.7 Å while the capture radius is 44.4 Å. Thus in 25% of the cross sectional area we use a somewhat smaller cross section than is valid. The effect on the rate would probably be less than 20% in the worst case.

The orbiting cross sections are[8]

$$\sigma_{13} = 2\pi \left(\frac{\alpha_{pol}\, e^2}{\mu_{13}}\right)^{1/2} \times \frac{1}{V_{13}} \qquad V_{13} = |\underset{\sim}{V}_1 - \underset{\sim}{V}_3| \tag{V.38}$$

and

$$\sigma_{23} = 2\pi \left(\frac{\alpha_{pol}\, e^2}{\mu_{23}}\right)^{1/2} \times \frac{1}{V_{23}} \qquad V_{23} = |\underset{\sim}{V}_2 - \underset{\sim}{V}_3| \tag{V.39}$$

where α_{pol} is the polarizability of the neutral, e is the electronic charge and μ is the ion-neutral reduced mass. Using Eqs. (V.24), (V.25), and (V.36) - (V.39), we can write

$$\int_{-\infty}^{\infty} dt\, \frac{V_{13}}{\lambda_1}\, \eta_1 = N2\pi \left(\frac{\alpha_{pol} e^2}{\mu_{13}}\right)^{1/2} \int_{-\infty}^{\infty} dt\, \eta_1 \tag{V.40}$$

$$= N4\pi \left(\frac{\alpha_{pol} e^2}{\mu_{13} V_{init}^2}\right)^{1/2} \left[\sqrt{R_1^2 + 2R_1 a - b^2} - a \cosh^{-1} \frac{R_1 + a}{\sqrt{a^2 + b^2}}\right]$$

where $a = e^2/2E = e^2/\mu V_{init}^2 = e^2/3kT$.

Substituting in Eq. (V.36) and integrating over b we obtain

$$\alpha = 8\pi^2 N \times$$

$$\left\{\left(\frac{\alpha_{pol} e^2}{\mu_{13}}\right)^{1/2} \left[\frac{(R_1^2 + 2R_1 a)^{3/2}}{3} - \frac{a^2 (R_1 + a)}{2} \left(\sqrt{\left(\frac{R_1 + a}{a}\right)^2 - 1} - \left(\frac{a}{R_1 + a}\right) \cosh^{-1}\left(\frac{R_1 + a}{a}\right)\right)\right]\right. \tag{V.41}$$

$$\left. + \left(\frac{\alpha_{pol} e^2}{\mu_{23}}\right)^{1/2} \left[\frac{(R_2^2 + 2R_2 a)^{3/2}}{3} - \frac{a^2 (R_2 + a)}{2} \left(\sqrt{\left(\frac{R_2 + a}{a}\right)^2 - 1} - \left(\frac{a}{R_2 + a}\right) \cosh^{-1}\left(\frac{R_2 + a}{a}\right)\right)\right]\right\}$$

Eq. (V.41) has the form

$$\alpha = \alpha^{o} N \qquad (V.42)$$

where α^{o} is independent of N and proportional to T^{-3}.

In Table XII the three body rate constants calculated from Eq. (V.41) are compared with the experimental rates obtained from Figs. 10-13. The experimental numbers represent the extrapolated zero pressure slope in those cases where the α vs N plots in Figs. 10-13 indicate a definite curvature at higher densities. The use of the orbiting cross sections in Eq. (V.36) is valid for all ion pairs in Table XII except for the complexed ions in argon, where the predicted rates may be as much as 50% too low. In view of the very poor agreement however, a numerical integration of Eq. (V.36) to include the effect of the "hard sphere" was not done. In all other cases the orbiting cross sections become equal to the average hard sphere cross sections at such small radii that the effect on the rate is less than 10%.

If we assume that the ions present in the experiment are complexed, as the previous chapter has indicated, the experimental results are up to 40 times higher than theory predicts for the case of xenon as a neutral and higher for the argon results. Furthermore, the predicted relative rates are not in accord with experiment.

The very low predictions of this model have been first pointed out by Brueckner in an analysis leading to Eq. (V.33) of the previous section (for the special case, $m_1 = m_2$). The previous agreement of experiment[9,10] must be considered fortuitous since the derivation of the capture radius used in the Thomson theory or the Nantanson modification cannot be justified.

Table XII

(a) Theoretical three body rates (α/N)			(b) Experimental three body rates (α/N)		
Ions	(Xe) $\alpha/N \times 10^{27}$ (cm^6/sec)	(Ar) $\alpha/N \times 10^{27}$ (cm^6/sec)	System	(Xe) $\alpha/N \times 10^{27}$ (cm^6/sec)	(Ar) $\alpha/N \times 10^{27}$ (cm^6/sec)
Tl^+, I^-	4.66	.995	TlI	30.4	13.0
Tl^+, Br^-	4.77	1.79	TlBr	19.6	10.6
Tl^+, Cl^-	4.10	4.25	TlCl	17.6	11.8
Tl^+, NO_3^-	6.44	3.34	$TlI\text{-}NO_2$	18.6	7.4
Tl_2^+I, TlI_2^-	.727	.0693			
Tl_2^+Br, $TlBr_2^-$	.765	.0813			
Tl_2^+Cl, $TlCl_2^-$	1.13	.143			
$Tl_2^+(NO_3)$, $Tl(NO_3)_2^-$	1.14	.129			

In a recent paper by Feibelman,[2] the three body ion-ion recombination rate at low density is studied using a Monte Carlo calculational method. In his paper Feibelman avoided the use of a capture radius and by the Monte Carlo method took proper account of averages of direction, velocity, and collision parameters. He found that by considering the effects of dissociative collisions and taking averages correctly the values of α turn out considerably larger than calculations based on the introduction of a capture radius. His computed values of α were within the experimental range for the O_2^+, O_2^- recombination data of Sayers.[9]

While the "brute force" method of Feibelman is useful in checking the validity of a proposed mechanism it is not easily adaptable for making routine predictions on three body recombination rates. At present, the mechanism appears to be adequate although better techniques are needed to take proper account of the collision dynamics. In particular, the effect of the velocity distribution, which has been completely neglected in the treatment based on a capture radius, may be important.

C. Two-Body Recombination

The two-body recombination process leading to mutual neutralization of a positive and a negative ion was illustrated schematically by Eq. (V.2). The transfer of an electron is generally an exothermic process and there are a number of modes in which the excess energy of the reaction may be absorbed: electronic excitation of either or both of the products, vibrational or rotational excitation if one or both of the species is a molecule, kinetic energy of relative motion of the neutralization products and further chemical processes other than simple electron transfer. Inelastic collisions between atomic systems are very difficult to describe mathematically and the situation in the case of

molecular ions is considerably more complex. We describe here only some qualitative features.

Because of the Franck-Condon principle the transition from one potential energy curve (or surface) to another takes place only if the curves (or surfaces) cross or come close together. As a result of the long range coulomb attraction between positive and negative ions the crossing of the potential energy curves of the X^+, Y^- system and the neutral species may occur at large internuclear separation leading to very large recombination cross sections $> 10^{-14}$ cm^2.

An example of the potential energy curves for the TlI molecule is given in Fig. 19. The atomic energy levels are taken from the tables of Moore.[11] The dissociation energy (2.79 ev)[12] and the ground state vibrational energy (150 cm^{-1}) (see Table VII) were used to fit the ground state to a Morse potential energy curve. The energy of the ions at infinite separation relative to the ground state atoms is equal to the difference between the ionization potential of thallium (6.11 ev)[13] and the electron affinity of iodine (3.06 ev).[14] The minimum in the ionic curve is approximated by the thallium iodide distance in the ionic crystal (see Table XI). All potential energy curves which lie above the ionic curve at infinity are not shown. Each of the potential energy curves in Fig. 19 except the ionic curve represent, at large internuclear separation, several degenerate electron terms. The energy levels are drawn in the first approximation. In higher approximations terms of the same symmetry, instead of crossing, only come close to one another.

A formula for the transition probability called the Landau-Zener formula was derived independently by Landau,[15] Zener,[16] and Stueckelberg.[17] The calculation of the transition probability according to the

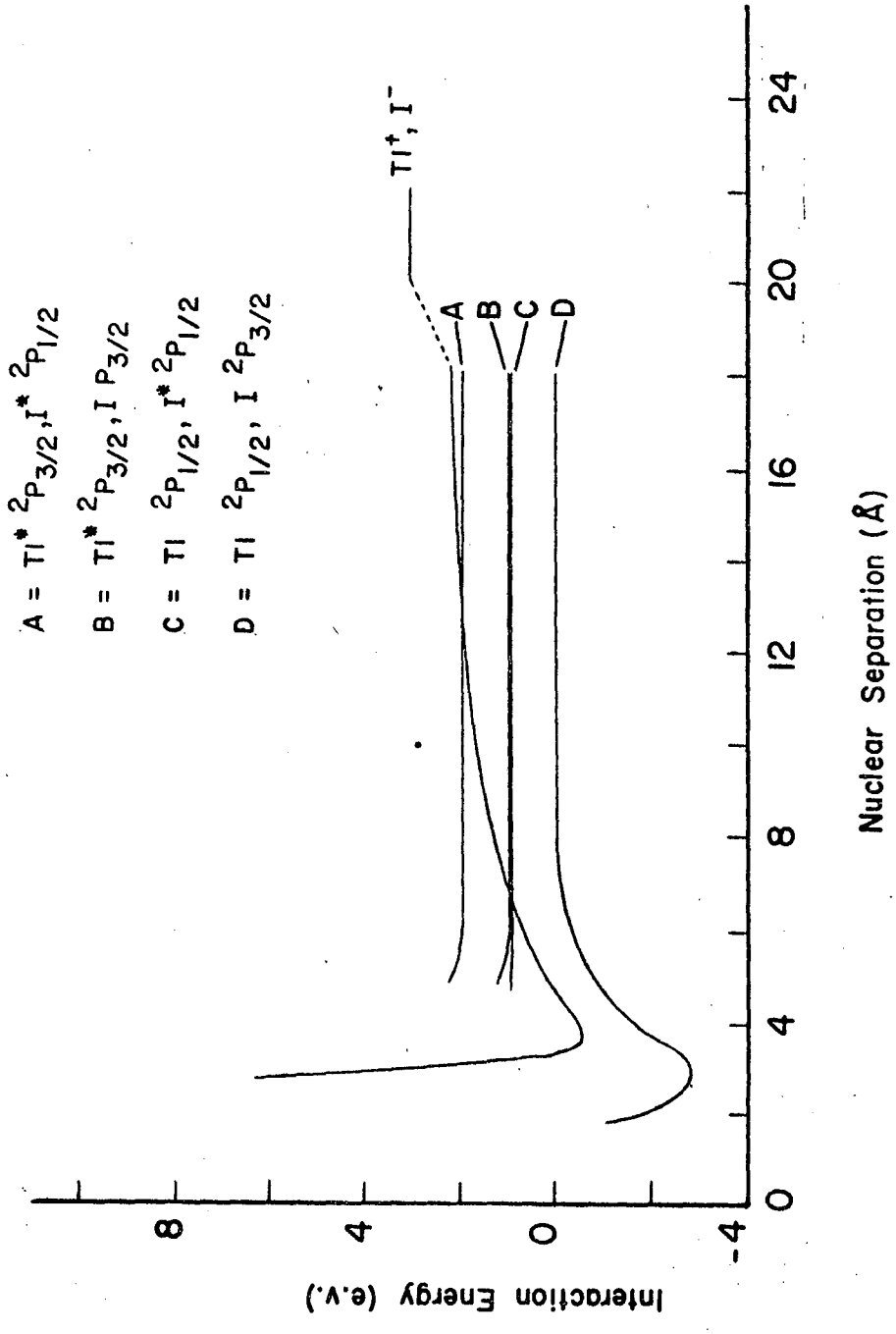

Fig. 19 Potential energy curves for TlI

Landau-Zener formula is prohibitively difficult except for very simple systems and furthermore, Bates[18] has shown that the formula is invalid over much of the energy region for which it was derived and to which it has been applied. One of the reasons for the failure of the formula is that, contrary to what is assumed, transitions may readily occur well away from the crossing point. This is especially true for intersections at large internuclear distances where the coulombic energy is changing very slowly (e.g. at 20 Å the coulombic energy change is ~ .04 ev/Å).

In the case of the molecular ions in our experiments the situation is more complex. The transition probability now depends on the rotational and vibrational state of the ions as well as their separation and speed, and we cannot even draw the potential curves at large separation (much less the complex potential energy surfaces at small internuclear separations) since, as pointed out in Chapter IV, the bond energy of the molecular ions can be estimated only very crudely. However, it is interesting to use the experimental rate constant (k_o), assume unit transition probability at some separation R and calculate the value of R necessary to give the required rate. The cross section for approach to a distance equal to or less than R is

$$\sigma = \pi b_c^2 = \pi R^2 \left(1 + \frac{e^2}{RE}\right) \qquad (V.43)$$

where b_c is the maximum value of the impact parameter which permits a distance of closest approach R, and E is the relative energy. Multiplying this cross section by the relative speed v and averaging over the Maxwell distribution gives

$$k_o = \langle \pi b_c^2 \, v \rangle = R^2 \left(\frac{8\pi kT}{\mu}\right)^{1/2} \left(1 + \frac{e^2}{RkT}\right) \qquad (V.44)$$

where μ is the reduced mass of the two ions. The values of k_o estimated from Figs. 10-13 and the values of R obtained from Eq. (V.44) are given in Table XIII Since we assumed a unit transition probability, the values of R in Table XIIIare really lower limits for the distance at which charge transfer does occur.

Table XIII Bimolecular recombination rates

System	$k_o \times 10^8$ ($cm^3 sec^{-1}$)	R (Å)
(Tl_2^+I, TlI_2^-)	4.0±.5	18
$(Tl_2^+Br, TlBr_2^-)$	5.1±.5	21.5
$(Tl_2^+Cl, TlBr_2^-)$	5.6±.7	22
$(Tl_2^+(NO_3), Tl(NO_3)_2^-)$	5.3±.5	21.5

If we assume the molecular ion curve crosses the ground state neutral curve at the value of R given in Table XIII, we can calculate the sum of the bond energies of the two complexes as the energy difference between the molecular ion curve and the atomic ion curve (except for $TlNO_3$ since the electron affinity of NO_3 is unknown). Half this value is the average bond energy for an ion pair and ranges from .92 ev for the pair $(Tl_2^+Cl, TlCl_2^-)$ to 1.12 ev for (Tl_2^+I, TlI_2^-). The relative bond energies for the complexes predicted in this way are the reverse of what is expected based on the estimates made in Chapter IV and their magnitudes are in general less than the values calculated there. Similar calculations based on the potential energy curves other than the ground state would predict a smaller bond energy.

In view of the above discussion it seems unlikely that the existence of a single crossing point with unit transition probability is an adequate descrption of the electron transfer process. A single crossing point at larger internuclear separation, several crossings, or just the close proximity of the ionic and neutral curves may be important. Because of the slow change in the coulombic energy with distance at large internuclear separations the interaction region may extend over a much wider range than previously thought. A large range of interaction may not be very sensitive to the precise crossing points and may be related to the fact that the R values given in Table XII differ so little. Until the bond energy of the complex is known with greater accuracy little progress can be made.

References for Chapter V

1. J. J. Thomson, Phil. Mag., 47, 337 (1924).
2. P. J. Feibelman, J. Chem. Phys. 42, 2462 (1965).
3. W. Machler, Z. Physik, 104, 1 (1936).
4. P. Langevin, Ann. Chim. Phys. 28, 289, 433 (1903).
5. G. L. Natanson, Soviet Phys.-Tech. Phys., 4, 1263 (1960).
6. K. A. Brueckner, J. Chem. Phys., 40, 439 (1964).
7. L. D. Landau and E. M. Lifshitz, Mechanics (Addison-Wesley, Reading, Mass., 1960), p. 38.
8. L. D. Landau and E. M. Lifshitz, Mechanics (Addison-Wesley, Reading, Mass., 1960), p. 51.
9. J. Sayers, Ionic Recombination, in Atomic and Molecular Processes, D. R. Bates, ed. (Academic Press, Inc., New York, 1962), p. 272.
10. B. H. Mahan and J. C. Person, J. Chem. Phys. 40, 392 (1964).
11. C. E. Moore, Atomic Energy Levels, Vol. III, Nat. Bur. Stand. Circ. 567, 1958.
12. D. Cubicciotti, J. Phys. Chem. 69, 1410 (1965).
13. V. I. Vedeneyev et al., Bond Energies Ionization Potentials and Electron Affinities (St. Martin's Press, New York, 1966).
14. R. S. Berry and C. W. Reimann, J. Chem. Phys. 38, 1540 (1963).
15. L. Landau, Z. Phys. Sowjet 2, 46 (1932).
16. C. Zener, Proc. Roy. Soc. A137, 696 (1932).
17. E. C. G. Stueckelberg, Helv. Phys. Acta 5, 369 (1932).
18. D. R. Bates, Proc. Roy. Soc. (London) A257, 22 (1960).

ACKNOWLEDGMENTS

This research was done under the direction of Professor Bruce H. Mahan. His encouragement, patience, and suggestions are very much appreciated.

I would also like to thank Charles Young for his assistance on numerous occasions and George Fisk for help in checking equations and for many useful discussions.

Also, I would like to acknowledge one year of support from I.B.M.

This work was done under the auspices of the United States Atomic Energy Commission.

This report was prepared as an account of Government sponsored work. Neither the United States, nor the Commission, nor any person acting on behalf of the Commission:

A. Makes any warranty or representation, expressed or implied, with respect to the accuracy, completeness, or usefulness of the information contained in this report, or that the use of any information, apparatus, method, or process disclosed in this report may not infringe privately owned rights; or

B. Assumes any liabilities with respect to the use of, or for damages resulting from the use of any information, apparatus, method, or process disclosed in this report.

As used in the above, "person acting on behalf of the Commission" includes any employee or contractor of the Commission, or employee of such contractor, to the extent that such employee or contractor of the Commission, or employee of such contractor prepares, disseminates, or provides access to, any information pursuant to his employment or contract with the Commission, or his employment with such contractor.